UNIMORE
UNIVERSITÀ DEGLI STUDI DI
MODENA E REGGIO EMILIA

Università degli Studi di Modena e Reggio Emilia
Facoltà di Medicina e Chirurgia

Corso di Laurea Magistrale in Medicina e Chirurgia

Dipartimento di Scienze Mediche e Chirurgiche, Materno-Infantili e dell'Adulto

Malattie dell'Apparato Respiratorio

Dynamic intrinsic PEEP in acute exacerbations of COPD: association with respiratory mechanics and their early response to high-flow nasal cannula — a physiological study

RELATORE:

Dr. Roberto Tonelli

CORRELATORE:

Prof. Enrico Clini

TESI DI LAUREA DI

Isacco Elredo Balbo

Anno Accademico 2025-2026

Table of Contents

Abstract **4**

Introduction **6**

Chronic obstructive pulmonary disease and its exacerbations *6*

Airway inflammation *7*

Mucus hypersecretion and muco-obstructive physiology *7*

Airflow limitation, air trapping, and dynamic hyperinflation *8*

Gas-exchange impairment and hypercapnia *9*

Respiratory muscle dysfunction and the load–capacity imbalance *10*

Effort-related lung stress *11*

Cardiopulmonary interactions *12*

Non-invasive respiratory support in hypercapnic ECOPD *12*

Assessment of inspiratory effort and respiratory muscle function *14*

Aim of the study *15*

Materials and methods **16**

Study design and population *16*

High-flow nasal cannula setting *17*

Study assessment protocol *17*

Signal acquisition and processing *17*

Inspiratory effort and its partitioning *18*

Nasal pressure swing *19*

Dynamic intrinsic PEEP and breathing pattern *20*

Respiratory muscle ultrasound *22*

Other measurements *24*

Study outcomes *24*

Statistical analysis *24*

Use of Artificial Intelligence Tools **25**

RESULTS **26**

Patient population *26*

Behaviour of physiological and clinical variables *29*

Baseline PEEPi,dyn and the cross-sectional physiological profile *34*

Baseline PEEPi,dyn and the early physiological response to HFNC *44*

DISCUSSION **54**

CONCLUSION **59**

References **60**

Abstract

Background

During exacerbations of COPD (ECOPD), dynamic intrinsic positive end-expiratory pressure (PEEPi,dyn) acts as an inspiratory threshold load, thereby increasing the work of breathing (1). High-flow nasal cannula (HFNC) is increasingly used in this setting (2); however, its ability to counteract PEEPi,dyn may be limited in patients with marked dynamic hyperinflation. The relationship between baseline PEEPi,dyn, respiratory mechanics, inspiratory effort partitioning, and their early physiological response to HFNC has not been characterized in spontaneously breathing patients with ECOPD.

Methods

In this prospective physiological study, spontaneously breathing patients with acute hypercapnic respiratory failure due to ECOPD underwent physiological assessment at HFNC initiation (T0) and after 2 h of standardized HFNC delivered at 40 L/min (T1). Measurements included dynamic intrinsic positive end-expiratory pressure (PEEPi,dyn), corrected for the abdominal contribution; esophageal (Pes), transdiaphragmatic (Pdi), and nasal (Pnose) pressure swings; esophageal and transdiaphragmatic pressure–time products (PTPes and PTPdi); maximal diaphragmatic pressure-generating capacity (Pdi,sniff); the Pes/Pdi ratio; respiratory muscle ultrasound indices; expiratory tidal volume (Vte), expressed as absolute values and normalized to predicted body weight (Vte/PBW); respiratory rate (RR); and dyspnea. Associations between baseline PEEPi,dyn and physiological variables at T0, as well as between baseline PEEPi,dyn and changes in these variables from T0 to T1, were explored using Spearman's rank correlation, with bootstrap 95% confidence intervals.

Results

Twelve patients underwent complete physiological assessment. At T0, higher PEEPi,dyn was associated with greater inspiratory effort, reflected by larger Pes and PTPes/min values (ρ=0.69 and 0.68) and larger Pdi and Pnose swings (ρ=0.69 and 0.82), and with lower maximal diaphragmatic pressure-generating capacity (Pdi,sniff; ρ=−0.77). At the same time point, higher PEEPi,dyn was also associated with a lower diaphragm thickening fraction (TF,di; ρ=−0.60), greater intercostal and sternocleidomastoid muscle recruitment (ρ=0.68 and 0.72), lower Vte and Vte/PBW (ρ=−0.80 and −0.69), and higher RR and dyspnea (ρ=0.71 and 0.61). Higher baseline PEEPi,dyn was associated with greater increases in Pes (ρ=0.69) and

PTPes/min (ρ=0.84) from T0 to T1, greater extra-diaphragmatic muscle recruitment, a reduction in Vte/PBW (ρ=−0.65), and persistence or worsening of PEEPi,dyn (ρ=0.76).

Conclusions

In spontaneously breathing patients with ECOPD treated with HFNC, higher PEEPi,dyn was associated with a respiratory mechanical pattern characterized by greater inspiratory effort and dyspnea, redistribution of inspiratory muscle activity, and lower tidal volume. Higher baseline PEEPi,dyn was also associated with a less favourable early physiological response to HFNC, characterized by greater inspiratory effort, increased extra-diaphragmatic muscle recruitment, less favourable changes in Vte/PBW, and persistence or worsening of PEEPi,dyn.

Introduction

Chronic obstructive pulmonary disease and its exacerbations

Chronic obstructive pulmonary disease (COPD) is a leading cause of morbidity and mortality worldwide and imposes a substantial and growing socioeconomic burden, with more than 200 million prevalent cases globally and a number of affected individuals projected to approach 600 million by 2050 (3,4). The Global Initiative for Chronic Obstructive Lung Disease (GOLD) defines an exacerbation of COPD (ECOPD) as an event characterized by an acute worsening of respiratory symptoms — dyspnea, cough, and sputum production — that usually lasts less than two weeks and requires additional therapy (5,6). Within the natural history of the disease, ECOPD are the events with the greatest short- and long-term prognostic impact, driving accelerated lung-function decline, hospitalization, and much of the morbidity, mortality, and healthcare cost attributable to COPD (7). Beyond their symptomatic burden, exacerbations represent major inflection points in the course of the disease: they worsen health-related quality of life, increase short- and long-term mortality, and exert systemic repercussions that extend well beyond the bronchial tree, involving immunological, metabolic, cardiovascular, and neuromechanical pathways (8,9). A relevant proportion of hospitalized patients develop acute hypercapnic respiratory failure, which reflects the inability of the respiratory pump to sustain the mechanical load imposed by the exacerbation and identifies a population at particularly high risk of adverse outcomes (7).

The pathobiology of ECOPD is inherently multidimensional. Airway and systemic inflammation, mucus hypersecretion and muco-obstructive disease, bronchoconstriction, ventilation–perfusion (V/Q) mismatch, dynamic hyperinflation, respiratory muscle overload, cardiopulmonary interactions, and effort-related mechanical stress collectively shape the clinical phenotype of the exacerbating patient (8). Rather than acting in isolation, these mechanisms reinforce one another in tightly interdependent loops, so that ECOPD is increasingly understood as a self-reinforcing cycle in which inflammatory, mechanical, and cardiovascular derangements amplify one another: airway inflammation, mucus hypersecretion, and bronchospasm intensify airflow limitation, which promotes air trapping and dynamic hyperinflation, increases the elastic and resistive loads on the respiratory muscles, and predisposes to respiratory-muscle dysfunction and, ultimately, ventilatory failure (8,9,10). A physiologically grounded understanding of these interactions is essential for clinical decision-making, including oxygen titration, bronchodilator use, assessment of inspiratory

effort, the choice and timing of non-invasive respiratory support, and the prevention of delayed escalation of care (8). The following paragraphs describe each of these mechanisms, with particular emphasis on those — dynamic hyperinflation, intrinsic positive end-expiratory pressure, and the load–capacity balance of the respiratory muscles — that are central to the present study.

Airway inflammation

Airway inflammation markedly increases during ECOPD and represents the dominant upstream driver of pathophysiological deterioration (8,9). Neutrophilic inflammation is the most prevalent pattern. Infectious stimuli — most commonly Haemophilus influenzae, Streptococcus pneumoniae, Moraxella catarrhalis, influenza virus, and rhinovirus — activate epithelial and innate immune pathways, triggering the recruitment and activation of neutrophils (9). These cells release interleukin (IL)-8, tumour necrosis factor-α, neutrophil elastase, proteases, and oxidants that promote epithelial injury, disrupt barrier integrity, and amplify mucus production, thereby perpetuating airflow obstruction, enhancing mucosal oedema, and impairing mucociliary clearance (8,11). Systemic inflammation, reflected by elevated C-reactive protein and leucocytosis, correlates with exacerbation severity and adverse outcomes (8). A clinically relevant subset of patients displays an eosinophilic or type-2–driven pattern, with increased IL-4, IL-5, and IL-13 activity; in these patients, blood eosinophil counts predict the response to inhaled corticosteroids and to biological agents targeting type-2 pathways (12). Importantly, the inflammatory endotype is not fixed but may shift over time in parallel with changes in the airway microbiome, underscoring the importance of longitudinal phenotyping (11). Overall, these inflammatory cascades act as a multilayer amplifier that shapes the downstream mechanical and gas-exchange consequences of ECOPD (8).

Mucus hypersecretion and muco-obstructive physiology

Airway mucus hypersecretion is a central contributor to airflow obstruction during ECOPD. Goblet cell hyperplasia and submucosal gland hypertrophy increase the synthesis of the gel-forming mucins MUC5AC and MUC5B, a process driven by chronic inflammation, epithelial injury, and type-2–mediated pathways (8,13). Submucosal glands, particularly abundant in the proximal airways, markedly amplify secretion in response to inflammatory and neural stimuli. Impaired mucus hydration and defective ion transport further increase mucus viscosity and elasticity, promoting adhesion of mucus to the airway walls and the formation of plaques and plugs (13). These plugs impair mucociliary clearance, foster local hypoxia and infection, and

generate regional V/Q mismatch (14). Large imaging cohorts have shown that the burden of mucus plugs on chest computed tomography is a strong and independent predictor of exacerbations and gas-exchange impairment; plugs may persist even in the absence of chronic bronchitis symptoms and are associated with lower FEV_1, greater dyspnea, and lower oxygen saturation (14,15). Muco-obstructive disease is therefore not merely a secondary finding but a primary pathogenic mechanism during ECOPD, and one that directly contributes to the increase in airway resistance and expiratory flow limitation described below (8).

Airflow limitation, air trapping, and dynamic hyperinflation

Acute worsening of airflow obstruction during ECOPD results from the combined effects of airway inflammation, bronchial smooth-muscle contraction, mucus plugging, and mucosal oedema (8,10). These processes reduce expiratory flow rates and prevent complete lung emptying, leading to progressive air trapping. Two components of hyperinflation should be distinguished. Static hyperinflation, driven by emphysema and loss of lung elastic recoil, chronically increases functional residual capacity; dynamic hyperinflation, in contrast, develops when tachypnea and increased ventilatory demand shorten expiratory time in the presence of expiratory flow limitation, so that each breath begins before the lung has returned to its relaxation volume (16,17).

From a mechanical standpoint, the worsening of expiratory flow limitation, the increase in airway resistance, and the loss of elastic recoil that characterize ECOPD prolong the expiratory time constant of the lung. When expiration is incomplete before the next inspiration begins, end-expiratory lung volume rises above the relaxation volume of the respiratory system and alveolar pressure remains positive at end-expiration, generating dynamic intrinsic positive end-expiratory pressure ($PEEPi,dyn$) (8,18). This positive end-expiratory alveolar pressure behaves as an inspiratory threshold load: the inspiratory muscles must first generate an equivalent amount of negative pressure to bring alveolar pressure below atmospheric level before inspiratory flow can begin, so that a substantial fraction of muscular effort is expended without contributing to tidal ventilation, thereby increasing the work of breathing (1,19). In patients with COPD, the portion of inspiratory work spent against this threshold load may be considerable and, in some conditions, exceed half of the total elastic work of breathing (20,21). Importantly, because the flow limitation of COPD is largely fixed, air trapping and $PEEPi,dyn$ are relatively refractory to a simple prolongation of expiratory time, which distinguishes this threshold load from that seen in purely restrictive conditions. Moreover, $PEEPi,dyn$ is not

determined by hyperinflation alone: recruitment of the expiratory (abdominal) muscles, which frequently accompanies increased ventilatory demand, can raise intrinsic PEEP independently of the degree of dynamic hyperinflation and, if not accounted for, can lead to an overestimation of the true inspiratory threshold load (22,23).

Dynamic hyperinflation has several additional detrimental consequences. It shifts the diaphragm to a flattened, mechanically inefficient position, increases the elastic load of inspiration, reduces inspiratory capacity, and markedly raises the work of breathing (8,16). As end-expiratory lung volume approaches total lung capacity, patients breathe on the upper, flat portion of the pressure–volume curve of the respiratory system, where small increases in tidal volume require disproportionately large pressure swings (24). Clinically, the degree of hyperinflation correlates more strongly with dyspnea and functional limitation than spirometric severity classes, emphasizing its central role in the ECOPD phenotype (17). Strategies such as bronchodilation, reduction of ventilatory demand, prolongation of expiratory time, and titration of external positive end-expiratory pressure during non-invasive ventilation may mitigate dynamic hyperinflation and its mechanical consequences (8,18).

Gas-exchange impairment and hypercapnia

Gas-exchange impairment is a defining feature of severe ECOPD and, in many patients, results in acute hypoxemic and hypercapnic respiratory failure (8,25). Hypoxemia arises primarily from V/Q mismatch: airway inflammation, bronchospasm, and mucus plugging reduce alveolar ventilation in regions where perfusion is preserved or even increased (26). The increased oxygen consumption of the respiratory muscles during ECOPD lowers mixed venous oxygen content and further worsens arterial oxygenation (26). Supplemental oxygen is therefore frequently required and should be carefully titrated to conservative saturation targets (5).

Hypercapnia derives from the convergence of several mechanical constraints (25,27). Expiratory flow limitation prevents complete lung emptying and increases dead-space ventilation, as a larger fraction of each breath ventilates poorly perfused, overdistended regions. The resulting dynamic hyperinflation flattens the diaphragm and places the inspiratory muscles at a mechanical disadvantage; as the load rises and efficiency declines, the ability to increase minute ventilation becomes limited. In parallel, the threshold load imposed by PEEPi,dyn requires patients to generate substantial negative pressure before inspiratory flow even begins, further reducing ventilatory efficiency. Patients consequently tend to adopt a rapid and shallow breathing pattern which, by increasing the ratio of dead space to tidal volume, further reduces

alveolar ventilation. Combined, these factors produce a state in which alveolar ventilation becomes insufficient for carbon dioxide clearance, leading to progressive hypercapnia and respiratory acidosis (25,27). Excessive oxygen administration may further aggravate hypercapnia by releasing hypoxic pulmonary vasoconstriction and redistributing perfusion toward poorly ventilated lung units (8,25). Hypercapnia is therefore a hallmark of ventilatory exhaustion. Beyond its role as a marker of pump failure, hypercapnia at admission has itself been associated with worse outcomes in hospitalized ECOPD, underscoring the clinical importance of the mechanical mechanisms that drive carbon dioxide retention (28).

Respiratory muscle dysfunction and the load–capacity imbalance

Respiratory muscle dysfunction is a pivotal determinant of clinical deterioration during ECOPD and a major contributor to hypercapnic respiratory failure (8,29). As airflow obstruction worsens, patients face a simultaneous rise in elastic load, due to breathing at high lung volumes; resistive load, due to narrowed airways; and threshold load, imposed by PEEPi,dyn (20,24). Dynamic hyperinflation does not only impose an added load; it simultaneously degrades the capacity of the pump that must overcome it. Lung-volume expansion shortens the diaphragm along its length–tension relationship, flattens its dome, and reduces the zone of apposition to the rib cage, placing the muscle at a marked mechanical disadvantage and curtailing its force- and pressure-generating capacity (30,31,32). At the cellular level, COPD is associated with structural and functional changes of the diaphragm fibres, including a reduced force-generating capacity per cross-sectional area, which further limit the reserve available when an acute load is superimposed (33). During exacerbations, systemic inflammation, oxidative stress, hypoxemia, and respiratory acidosis further impair muscle contractility and accelerate fatigue (29). Consistently, a reduction of maximal diaphragmatic pressure-generating capacity has been documented as COPD transitions from the stable state to an acute exacerbation with respiratory failure (34).

Under these conditions, increases in neural respiratory drive no longer translate into proportional increases in tidal volume, a hallmark of neuromechanical uncoupling (35,36). As diaphragmatic reserve is eroded, ventilatory demand is progressively met through greater recruitment of the extra-diaphragmatic and accessory inspiratory muscles, namely the parasternal intercostals, the scalenes, and the sternocleidomastoids (37,38). The parasternal intercostals are obligatory inspiratory muscles whose activity rises with inspiratory load, and patients with COPD show increased parasternal intercostal and scalene activation, consistent

with their heightened contribution to rib-cage expansion when the diaphragm is mechanically disadvantaged (37,38). The sternocleidomastoid, in contrast, is recruited later, as inspiratory effort increases and lung volume rises, so that its activation marks an advanced compensatory state (30,39). These muscles are less efficient and more metabolically costly than the diaphragm: their recruitment increases the oxygen cost of breathing while contributing comparatively little to effective alveolar ventilation (8). This redistribution of effort, together with recruitment of the expiratory muscles, may in turn further compress expiratory flow and aggravate gas trapping, pointing to a bidirectional interaction between dynamic hyperinflation and respiratory-muscle activity rather than a unidirectional cause-and-effect relationship (23,40). Once fatigue ensues, patients develop rapid shallow breathing, rising $PaCO_2$, and a downward spiral toward ventilatory pump failure (8,27).

The consequences of this load–capacity imbalance extend from mechanics to symptoms. When the neural drive to breathe increases but the mechanically constrained respiratory system cannot translate that drive into a proportionate ventilatory output, a neuromechanical dissociation arises that is a principal determinant of the intensity of dyspnea in COPD (35,36). Clinically, greater dynamic hyperinflation and inspiratory loading have therefore been associated with a heavier dyspnea burden, greater disease severity, and worse outcomes (17,41). In hospitalized patients with ECOPD, neural respiratory drive has also been shown to track clinical deterioration and recovery, supporting the value of physiological markers of the load–capacity balance for bedside monitoring (42).

Effort-related lung stress

Although patient self-inflicted lung injury (P-SILI) was initially conceptualized in acute hypoxemic respiratory failure, the physiology of ECOPD suggests a plausible and clinically relevant variant: effort-related lung stress driven by severe expiratory flow limitation, hyperinflation, and high inspiratory drive (8). During exacerbations, the combination of airway obstruction and PEEPi,dyn forces patients to generate large negative pleural pressure swings to initiate and sustain inspiratory flow (19,21). These exaggerated pleural pressure oscillations translate into large transpulmonary pressure swings, which are recognized mediators of regional lung stress and strain (43). COPD lungs are intrinsically heterogeneous, with emphysematous regions coexisting next to relatively preserved units, and vigorous spontaneous efforts may amplify this heterogeneity, particularly at compliance gradients where shear forces are greatest. These forces may promote regional overdistension, cyclical opening

and closing of unstable units, increased microvascular pressure gradients and, through pendelluft, an out-of-phase redistribution of gas between lung regions that increases local deformation beyond what bulk tidal volume would suggest (8). Although direct clinical evidence is still limited, this physiology suggests a self-reinforcing cycle that may worsen V/Q mismatch and fuel local inflammation. Early control of excessive inspiratory effort — through bronchodilation, external positive end-expiratory pressure, or non-invasive ventilation — may therefore serve not only to improve ventilation but also to limit effort-related mechanical injury (8,43), further supporting the importance of quantifying inspiratory effort in spontaneously breathing patients with ECOPD.

Cardiopulmonary interactions

ECOPD also affects the cardiovascular system through intertwined mechanical, haemodynamic, autonomic, and inflammatory pathways (8). A characteristic change is an acute rise in pulmonary vascular resistance, driven by hypoxic pulmonary vasoconstriction, airway inflammation, endothelial dysfunction, and dynamic hyperinflation. In COPD, chronic hypoxia, oxidative stress, and impaired nitric-oxide signalling blunt the efficacy of hypoxic pulmonary vasoconstriction, so that during exacerbations widespread regional hypoxia produces an exaggerated yet inefficient vasoconstrictive response that worsens V/Q mismatch (8,26). Haemodynamically, ECOPD substantially increases right ventricular afterload: echocardiographic studies show increased pulmonary artery pressures and transient right ventricular dysfunction during exacerbations, and even modest pressure elevations may unmask latent right ventricular impairment (44). Through ventricular interdependence, right ventricular strain alters left ventricular mechanics, as septal shift and large intrathoracic pressure swings impair left ventricular filling, reducing preload and limiting cardiac output precisely when metabolic demand rises (19,44). Dynamic hyperinflation and PEEPi,dyn further reduce venous return, amplifying this preload limitation (19). Finally, systemic inflammation, endothelial dysfunction, and autonomic imbalance promote a prothrombotic state; myocardial injury, arrhythmias, and heart-failure decompensation are more frequent during and immediately after an exacerbation, and cardiac biomarkers such as natriuretic peptides and troponins frequently rise even in the absence of overt ischaemia (8,44).

Non-invasive respiratory support in hypercapnic ECOPD

Non-invasive ventilation (NIV) remains the first-line respiratory support for acute hypercapnic COPD exacerbations with respiratory acidosis precisely because it addresses both sides of this

imbalance: externally applied positive end-expiratory pressure can partially counterbalance PEEPi,dyn and reduce the inspiratory threshold load, while inspiratory pressure support directly unloads the respiratory muscles, improves neuromechanical coupling, and restores the ability to generate adequate tidal ventilation (18,45). In parallel, high-flow nasal cannula (HFNC) has emerged as an alternative or complementary support strategy, and its use in hypercapnic patients has grown considerably (2). Its physiological benefits include washout of upper-airway dead space with improved ventilatory efficiency and carbon dioxide clearance, delivery of warmed and humidified gas that reduces inspiratory resistance and may limit bronchoconstriction, generation of a low and flow-dependent level of positive airway pressure, a reduction in respiratory rate with consequent lengthening of expiratory time, and generally good patient tolerance (46,47). Nonetheless, current European Respiratory Society guidelines suggest a trial of NIV before HFNC in patients with COPD and acute hypercapnic respiratory failure, with HFNC being considered in selected, less severe cases or in patients who do not tolerate NIV (48).

The magnitude of external positive pressure produced by HFNC is modest and strongly dependent on flow, cannula fit, and mouth opening (49,50), and may be insufficient to counterbalance PEEPi,dyn in patients with pronounced dynamic hyperinflation. In hypercapnic COPD, the ventilatory effectiveness of nasal high flow has been shown to depend on the delivered flow rate and on leakage around the cannula (51). Consistent with this, physiological work indicates that HFNC reduces the metabolic work of breathing (effort per minute) but is less effective than NIV at unloading the respiratory muscles on a breath-by-breath basis (52,53). Clinically, the evidence is correspondingly nuanced: while some trials report favourable effects of HFNC on carbon dioxide clearance, dyspnea, and comfort (54), a recent randomized trial failed to demonstrate non-inferiority of HFNC to NIV in moderate hypercapnic COPD exacerbations (55), another randomized non-inferiority trial in hypercapnic ECOPD reached partly different conclusions (56), and the larger RENOVATE trial found HFNC non-inferior to facemask NIV for a composite of intubation or death across mixed causes of acute respiratory failure (57). Because the inspiratory threshold load may account for more than half of the total work of breathing in this population (20), the physiological response to HFNC in ECOPD is likely to be heterogeneous and critically dependent on the magnitude of the underlying PEEPi,dyn. In line with this, HFNC has been shown to be less effective in reducing inspiratory effort when baseline effort is moderate to high in acute hypoxemic

respiratory failure (58), and in patients with ECOPD who failed an HFNC trial, inspiratory effort and accessory muscle recruitment were already increased at treatment initiation (41).

Assessment of inspiratory effort and respiratory muscle function

Although the relationship between PEEPi,dyn and respiratory mechanics has been described in stable COPD (59) and in mechanically ventilated patients (60), it has not been characterized during spontaneous breathing in the acute phase of ECOPD, where the interplay between threshold load, effort partitioning, and the response to a specific support such as HFNC is most clinically relevant. Esophageal and transdiaphragmatic pressure monitoring remains the reference standard for quantifying inspiratory effort, its partitioning among the respiratory muscles, and PEEPi,dyn, enabling direct assessment of respiratory mechanics and of the pressure–time products that integrate the intensity and duration of muscular contraction (61,62). In spontaneously breathing patients, PEEPi,dyn is measured as the esophageal pressure deflection that precedes the onset of inspiratory flow; because expiratory muscle relaxation at the beginning of inspiration may contribute to this deflection, concurrent recording of gastric pressure is required to correct for the abdominal contribution (22,23). The prognostic relevance of early effort assessment has been shown in de novo acute respiratory failure, where the lack of reduction in esophageal pressure swings within the first two hours of NIV predicted treatment failure (63). Despite its physiological value, however, esophageal manometry has not been widely adopted in clinical practice because of its invasiveness, cost, and the specialized expertise required for accurate interpretation (62,64).

In response to these limitations, non-invasive surrogates of inspiratory effort have been developed. Nasal pressure swing (Pnose), recorded through a pressure line sealed in one nostril while the contralateral nostril receives the high-flow gas, closely tracks esophageal pressure swings during HFNC, esophageal swings being approximately 2.2-fold larger than the corresponding Pnose values (65). In acute hypoxemic respiratory failure, a Pnose above 5.1 cmH_2O two hours after HFNC initiation identified patients at higher risk of early HFNC failure (66), and an elevated Pnose was independently associated with a lower probability of being alive and free from respiratory support at day 7 (67).

In parallel, respiratory muscle ultrasound (US) offers a bedside, radiation-free assessment of inspiratory muscle activity. The diaphragm thickening fraction (TF,di), measured at the zone of apposition, has been validated as an index of diaphragmatic contractile activity (68), and US-assessed diaphragmatic impairment predicts NIV failure and mortality in patients with

ECOPD (69). The diaphragm, however, is only one component of the inspiratory pump. US assessment of the parasternal intercostal muscles has been validated in mechanically ventilated patients as a feasible and reproducible index of extra-diaphragmatic recruitment (70,71), and the ratio between parasternal intercostal and diaphragm thickening fractions has been proposed as a marker of compensatory activation in COPD (72). Similarly, US of the sternocleidomastoid has revealed structural adaptations of this muscle in COPD (73). During assisted ventilation, increases in inspiratory effort measured by esophageal manometry have been accompanied by a relative reduction of TF,di and a proportionally greater parasternal intercostal activation (74), and in patients with ECOPD treated with HFNC, lower TF,di and greater intercostal and sternocleidomastoid recruitment were associated with higher Pnose, worse gas exchange, and HFNC failure (41). Notably, in hyperinflated patients TF,di may correlate poorly with transdiaphragmatic pressure (75,76), so that ultrasound- and pressure-derived indices should be regarded as complementary rather than interchangeable. Together, Pnose and respiratory muscle US provide complementary bedside information on the magnitude of inspiratory effort and on the shift of activity from the diaphragm toward the accessory muscles, and may help translate these physiological concepts into more readily applicable monitoring.

Aim of the study

Against this background, we conducted a prospective physiological study in spontaneously breathing patients with ECOPD to investigate the relationship between PEEPi,dyn, respiratory mechanics, and inspiratory-effort partitioning at baseline, as well as their early evolution over the first hours of HFNC. We hypothesized that higher PEEPi,dyn would be associated, at baseline, with greater inspiratory effort, a shift of inspiratory effort away from the diaphragm toward the extra-diaphragmatic muscles, increased accessory-muscle recruitment, a less favourable breathing pattern, and more severe dyspnea, and that it would identify patients with a less favourable mechanical response during the first 2 hours of HFNC.

Materials and methods

Study design and population

This was a prospective, single-centre physiological study conducted in the Respiratory Intermediate Care Unit of the University Hospital of Modena, Italy, between July 1st, 2025, and July 1st, 2026. Consecutive adult patients admitted with an acute exacerbation of chronic obstructive pulmonary disease (ECOPD) and deemed suitable for an initial trial of high-flow nasal cannula (HFNC) according to the institutional protocol were screened for enrolment. COPD was defined according to the Global Initiative for Chronic Obstructive Lung Disease (GOLD) criteria, based on a compatible clinical history and risk-factor exposure together with a documented post-bronchodilator $FEV_1/FVC < 0.70$ (5). An acute exacerbation was defined as an acute worsening of respiratory symptoms beyond normal day-to-day variation and requiring a change in regular therapy (5).

Patients were eligible if they presented with acute hypercapnic respiratory failure secondary to ECOPD accompanied by mild-to-moderate respiratory acidosis (arterial pH 7.25–7.35), preserved consciousness, no signs of severe respiratory distress, and no indication for immediate ventilatory assistance. Patients requiring immediate ventilatory support because of severe acidosis ($pH < 7.25$), altered mental status, severe respiratory distress, or other signs of clinical instability were not considered eligible for an HFNC trial.

Exclusion criteria were: inability to cooperate with physiological measurements; intolerance to HFNC; pregnancy; neuromuscular disorders affecting the respiratory muscles; interstitial lung disease; known diaphragmatic dysfunction unrelated to COPD (e.g., hemidiaphragm paralysis or surgical phrenic nerve injury); and refusal to participate in the study or to undergo esophageal catheter placement.

At enrolment, demographic and anthropometric characteristics, comorbidities, background inhaled therapy, and exposure to systemic corticosteroids within the previous 6 months were recorded. All enrolled patients received standard medical treatment for ECOPD in accordance with current international guidelines, including bronchodilators, systemic corticosteroids, antibiotics when clinically indicated, and controlled oxygen supplementation (5). The study was approved by the local Ethics Committee (protocol number 165/2024/SPER/AOUMO, SIRER ID 7354), and written informed consent was obtained from all participants before enrolment.

High-flow nasal cannula setting

HFNC was delivered through the AIRVO™ 2 system (Fisher & Paykel Healthcare, Auckland, New Zealand), a device incorporating a flow generator and a heated humidifier, using standard symmetric nasal cannulae. Gas flow was standardized at 40 L/min with a gas temperature of 37 °C, and the fraction of inspired oxygen (FiO_2) was titrated to maintain peripheral oxygen saturation between 92% and 94%. The same flow and temperature settings were maintained unchanged between T0 and T1, so that any change in the physiological variables could not be attributed to a modification of the HFNC settings. Throughout the study period, patients were continuously monitored, and escalation to non-invasive ventilation was decided by the attending physician according to predefined institutional criteria, including worsening respiratory acidosis or a rise in $PaCO_2$, persistent or worsening hypoxemia, respiratory rate > 25 breaths/min, progressive or unrelieved dyspnea, and clinical signs of increased work of breathing (41).

Study assessment protocol

Each patient underwent a comprehensive physiological assessment at two predefined time points: at HFNC initiation (T0, baseline) and after 2 hours of standardized HFNC treatment (T1). At both time points, the assessment comprised measurements of inspiratory effort and its partitioning among the respiratory muscles, respiratory mechanics and breathing pattern, respiratory muscle ultrasound, arterial blood gas analysis, and dyspnea. Patients were studied in the semi-recumbent position, and the measurements were acquired in the same fixed sequence at both time points: respiratory muscle ultrasound and Pnose were recorded first, during ongoing HFNC; a brief standardized interruption of HFNC was then performed to measure PEEPi,dyn, expiratory tidal volume, and Pdi,sniff, after which HFNC was immediately resumed.

Signal acquisition and processing

Esophageal (Pes) and gastric (Pga) pressures were measured with a double-balloon nasogastric catheter (NutriVent®, SIDAM, Mirandola, Italy) connected to a dedicated pressure-monitoring system (OptiVent®, SIDAM, Mirandola, Italy). The catheter was inserted transnasally according to standard procedures. Correct positioning of the esophageal balloon was verified by the presence of cardiac oscillations on the Pes tracing and confirmed by chest radiography showing the radiopaque markers at the appropriate anatomical level, whereas gastric balloon positioning was verified by the expected positive pressure deflection during gentle manual

abdominal compression. Because the esophagus lies within the pleural space, changes in Pes reflect changes in pleural pressure, and esophageal pressure was therefore used as the bedside surrogate of pleural pressure to quantify the magnitude and partitioning of inspiratory effort; Pga, in turn, was used as a surrogate of abdominal pressure (61,62).

Airflow, Pes, and Pga were acquired synchronously by a single OptiVent® unit and digitized through a common analog-to-digital converter at 100 Hz, ensuring intrinsic temporal alignment across channels. During acquisition, flow and Pes were displayed in real time to monitor the PEEPi,dyn interval, while flow, Pes, and Pga were recorded simultaneously and exported via USB for offline analysis. All derived variables were computed post hoc from these co-registered raw signals, with breath-by-breath reconstruction and superimposition of flow, Pes, and Pga on a common time axis, so that no additional bedside measurement was required.

For each measurement epoch, at least three consecutive stable, artefact-free respiratory cycles were selected and averaged. Cycles affected by swallowing, coughing, movement artefacts, cardiogenic-oscillation–dominated segments, signal instability, or baseline drift were excluded. This same set of selected breaths was used for all pressure-, timing-, and flow-derived indices.

Inspiratory effort and its partitioning

Tidal inspiratory Pes was calculated as the difference between the end-expiratory value and the inspiratory nadir of the esophageal pressure signal (77). Transdiaphragmatic pressure (Pdi) was obtained as the instantaneous difference between Pga and Pes, and tidal Pdi was defined as the inspiratory swing from end-expiration to peak inspiration; because the diaphragm separates the thoracic and abdominal compartments, Pdi specifically reflects the pressure generated by diaphragmatic contraction, whereas Pes reflects the pressure generated by all inspiratory muscles acting on the lung (61,77). Inspiratory effort was additionally quantified as the pressure–time products of the esophageal (PTPes) and transdiaphragmatic (PTPdi) pressures, computed by integrating the respective pressure signals over the neural inspiratory time — from the onset of inspiratory effort to the peak inspiratory pressure, relative to the end-expiratory baseline — and expressed both per minute and per breath. Unlike pressure swings, pressure–time products integrate both the intensity and the duration of muscular contraction, and their minute values are closely related to the metabolic cost of breathing (77). The Pes/Pdi ratio was derived from the tidal inspiratory swings of Pes and Pdi as an index of the relative contribution of the extra-diaphragmatic versus diaphragmatic muscles to inspiratory effort.

Throughout the manuscript, Pes, Pdi, and Pnose denote tidal inspiratory pressure swings unless otherwise specified.

Maximal diaphragmatic pressure-generating capacity (Pdi,sniff) was assessed using repeated maximal sniff maneuvers initiated from functional residual capacity, with patients instructed to perform short, sharp inspiratory efforts through the nose. At least three technically acceptable maneuvers were obtained, and the highest value was retained for analysis.

Nasal pressure swing

Nasal pressure swing (Pnose) was measured non-invasively with a custom-made nasal pressure monitoring system, according to a standardized protocol previously described and validated by our group (65,66,67). The system consists of a hypoallergenic, soft, self-expanding foam plug (3M Company, Saint Paul, MN, USA) through which a 16-gauge polyurethane intravenous cannula is inserted, the cannula acting as the pressure-sensing line. After compression, the foam plug was inserted into one nostril, alongside the NutriVent® catheter, where its re-expansion created an airtight seal; the contralateral nostril remained patent and received the HFNC prong, so that high-flow delivery continued throughout the measurement (65,67). The cannula was connected through a pressure line to the same monitoring system (OptiVent®, SIDAM, Mirandola, Italy) used for Pes and Pga. With the nostril sealed and the mouth closed, the pressure recorded in the occluded nostril reflects the nasopharyngeal pressure changes generated by inspiratory effort (65).

Pnose was recorded during ongoing HFNC, immediately before the HFNC interruption, with the patient in the semi-recumbent position with the head slightly tilted forward and the mouth closed, during quiet spontaneous breathing for approximately 3 minutes; the whole session, including set-up and data acquisition, lasted approximately 5–10 minutes (67). Pnose was defined as the tidal inspiratory swing of nasal pressure, i.e., the difference between the end-expiratory value and the inspiratory nadir of the nasal pressure signal, consistently with the definition adopted for Pes. Pressure waveforms were visually inspected before analysis; cycles affected by swallowing, coughing, movement artefacts, signal instability, or baseline drift were excluded, and measurements were obtained offline by averaging at least three consecutive stable respiratory cycles.

In the original validation study, Pnose showed a close relationship with Pes in spontaneously breathing patients receiving HFNC, esophageal pressure swings being approximately 2.2-fold larger than the corresponding Pnose values (65). Previous studies have also shown that

occlusion of one nostril during the measurement has a minimal influence on the flow and pressure delivered by HFNC and does not significantly affect the reliability of the measurement (51,65,66).

Dynamic intrinsic PEEP and breathing pattern

Dynamic intrinsic positive end-expiratory pressure (PEEPi,dyn) and expiratory tidal volume (Vte) were measured during a brief, standardized interruption of HFNC not exceeding two minutes, with a flanged mouthpiece and nose clip in place, after which HFNC was immediately resumed. Recording began immediately after removal of the nasal cannulae, without a washout period, to limit dissipation of the physiological conditions established during HFNC.

PEEPi,dyn was defined as the negative Pes deflection between the onset of inspiratory effort — identified on the Pes signal as the departure from the end-expiratory value — and the zero-flow point, identified on the flow signal as the transition from expiratory to inspiratory flow. This deflection represents the pressure that the inspiratory muscles must generate to offset the positive end-expiratory alveolar pressure before inspiratory flow can begin (1,19). To account for the abdominal (expiratory muscle) contribution to the esophageal deflection, PEEPi,dyn was corrected using the gastric pressure total decay (Pga,decay) method: Pga,decay was measured on the co-registered Pga signal as the fall in Pga from its end-expiratory value to its inspiratory nadir — which may occur after the onset of inspiratory flow — and corrected PEEPi,dyn was computed breath-by-breath as uncorrected PEEPi,dyn minus Pga,decay (Figure 1) (22). This correction is required because relaxation of expiratory muscles recruited during the preceding expiration lowers pleural pressure at the beginning of inspiration independently of inspiratory muscle activity, so that the uncorrected Pes deflection may overestimate the true inspiratory threshold load (22,23). Expiratory gastric pressure rise (Pga,rise), reflecting expiratory (abdominal) muscle activity, was defined as the increase in Pga from the onset of expiration to its end-expiratory peak.

Vte was obtained by digital integration of the expiratory flow signal and expressed both as an absolute value and normalized to predicted body weight (Vte/PBW). From the flow signal, inspiratory time (Ti), total breath duration (Ttot), duty cycle (Ti/Ttot), respiratory rate (RR = 60/Ttot), and mean inspiratory flow (Vte/Ti) were derived.

Figure 1. Correction of dynamic intrinsic positive end-expiratory pressure for gastric pressure total decay.

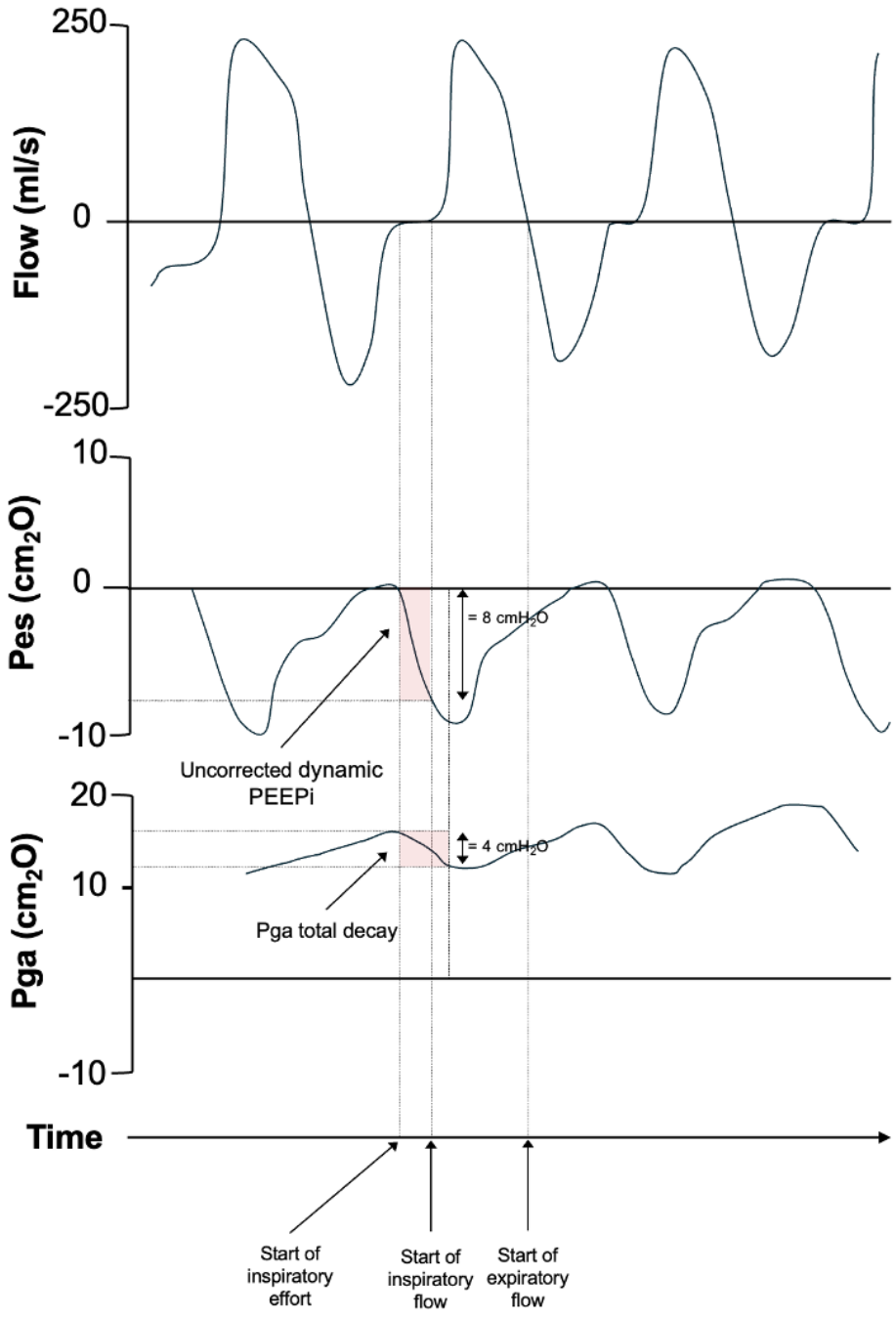


Figure 1. Representative tracings of respiratory flow, esophageal pressure (Pes), and gastric pressure (Pga) illustrating the measurement and correction of dynamic intrinsic positive end-expiratory pressure (PEEPi,dyn). The onset of inspiratory effort is identified by the initial negative deflection in Pes, whereas the onset of inspiratory flow occurs later, when flow crosses zero. Uncorrected PEEPi,dyn is estimated as the decrease in Pes between the onset of

inspiratory effort and the onset of inspiratory flow (8 cmH_2O in the illustrated example). Because expiratory muscle relaxation may contribute to the Pes deflection and thereby overestimate the true inspiratory threshold load, PEEPi,dyn is corrected using the Pga total decay method. Pga total decay is measured as the decrease from the end-expiratory Pga value to its subsequent nadir during inspiration (4 cmH_2O in the example), which may occur after the onset of inspiratory flow. Corrected PEEPi,dyn is calculated as uncorrected PEEPi,dyn minus Pga total decay, yielding 4 cmH_2O in the illustrated example. Vertical dotted lines indicate, from left to right, the onset of inspiratory effort, onset of inspiratory flow, and onset of expiratory flow. Shaded areas highlight the pressure changes used to derive uncorrected PEEPi,dyn and Pga total decay.

Abbreviations

Pes, esophageal pressure; Pga, gastric pressure; PEEPi,dyn, dynamic intrinsic positive end-expiratory pressure.

Respiratory muscle ultrasound

Respiratory muscle ultrasound (US) was performed by a single operator experienced in respiratory muscle imaging, during ongoing HFNC and immediately before the HFNC interruption, with the patient in the semi-recumbent position (head of the bed elevated at approximately 30°) and breathing spontaneously. A high-frequency linear transducer (7.5–15 MHz) was used for all muscles, which were examined sequentially — diaphragm, parasternal intercostal, and sternocleidomastoid — in a standardized order, to ensure consistent acquisition and minimize variability (41). A complete examination of the three muscles required approximately 10 minutes.

Diaphragm. The right hemidiaphragm was examined in B-mode at the zone of apposition, with the transducer placed between the 8th and 10th intercostal spaces along the mid-axillary line, using the liver as an acoustic window (41,68). At this site, the diaphragm appears as a trilaminar structure, consisting of a hypoechoic muscular layer bounded by two hyperechoic lines, the parietal pleura superficially and the peritoneum deeply; diaphragm thickness (Tdi) was measured between these two lines (68). Tdi was measured at end-expiration (Tdi,exp) and at peak inspiration (Tdi,insp) during tidal breathing, and the diaphragm thickening fraction (TF,di) was calculated as (68):

$$\mathbf{TF,di = [(Tdi,insp - Tdi,exp) / Tdi,exp] \times 100}$$

Maximal diaphragmatic recruitment was assessed during a maximal sniff manoeuvre initiated from functional residual capacity, with the transducer maintained in the same position. The diaphragmatic recruitment index (TMax,di) was calculated as the ratio between diaphragm thickness at peak inspiration during tidal breathing and diaphragm thickness at peak inspiration during maximal sniff (78):

$$\mathbf{TMax,di = Tdi,insp,tidal / Tdi,insp,sniff}$$

Parasternal intercostal muscle. The parasternal intercostal muscle was examined at the level of the second intercostal space, 3–6 cm lateral to the sternal edge, with the transducer oriented in a sagittal plane so as to visualize the second and third ribs and the intervening intercostal space (70,71). The muscle belly was identified in B-mode, deep to the pectoralis major muscle, between the superficial and deep fascial layers; M-mode was then used to track the dynamic changes in muscle thickness during tidal breathing, and parasternal intercostal thickness (Tic) was measured at end-expiration and at end-inspiration (41,71).

Sternocleidomastoid muscle. The sternocleidomastoid was examined with the transducer placed transversely at the mid-belly of the muscle, approximately halfway between the mastoid process and the clavicle and lateral to the carotid sheath. The muscle was visualized between the superficial and prevertebral fasciae, and its thickness (Tscm) was measured in M-mode at end-expiration and at peak inspiratory contraction (41,73).

The thickening fractions of the parasternal intercostal (TF,ic) and sternocleidomastoid (TF,scm) muscles were calculated with the same formula adopted for the diaphragm (70), as previously applied in this population (41):

$$\mathbf{TF,ic = [(Tic,insp - Tic,exp) / Tic,exp] \times 100}$$

$$\mathbf{TF,scm = [(Tscm,insp - Tscm,exp) / Tscm,exp] \times 100}$$

For all muscles, three consecutive respiratory cycles were recorded and averaged to reduce intra-observer variability. Measurements were acquired exclusively during quiet tidal breathing, avoiding voluntary deep breaths, sighs, coughing, and speech. Probe position and machine settings were kept constant throughout each session, and the same acoustic windows were used at T0 and T1 to ensure comparability between time points (41). Images with inadequate visualization or motion artefacts were discarded before analysis. Respiratory muscle US has shown good intra- and inter-observer reproducibility in this setting (79,80).

Other measurements

Dyspnea was graded with the modified Borg scale, a 0–10 category-ratio scale on which patients rated the intensity of their breathlessness from 0 (nothing at all) to 10 (maximal). Arterial blood gas analysis (pH, $PaCO_2$, PaO_2, bicarbonate, base excess, and lactate), with calculation of the PaO_2/FiO_2 ratio, was performed at both T0 and T1, together with the recording of heart rate, mean arterial pressure, and Glasgow Coma Scale. All tidal pressure-, flow-, and timing-derived indices were obtained from the same signals recorded during the standardized HFNC interruption and averaged over at least three stable, artefact-free respiratory cycles; Pdi,sniff was measured during the same interruption, retaining the highest value. US-derived indices and Pnose were acquired immediately before the interruption, during ongoing HFNC.

Study outcomes

The primary outcome was the relationship between baseline PEEPi,dyn and the magnitude of inspiratory effort, quantified as tidal Pes; PTPes/min was analysed as a confirmatory index. Secondary outcomes explored the relationship between baseline PEEPi,dyn and the broader physiological respiratory profile at T0, examined according to a pre-specified hierarchy:

1. **Inspiratory effort partitioning and diaphragmatic mechanics:** Pdi and PTPdi/min, Pnose, Pdi,sniff, Pga,rise, Pes/Pdi ratio, PTPes/breath, and PTPdi/breath.
2. **Respiratory mechanics and breathing pattern:** Vte (absolute and normalized to PBW), RR, and inspiratory timing (Ti, Ti/Ttot, Vte/Ti).
3. **Ultrasound-assessed respiratory muscle recruitment:** TF,di, TMax,di, TF,ic, and TF,scm.
4. **Dyspnea:** modified Borg score.

A further secondary outcome was the relationship between baseline PEEPi,dyn and the early physiological response to HFNC, quantified as the T0–T1 change in the above variables over the first 2 hours of treatment, following the same hierarchical structure.

Statistical analysis

Given the exploratory physiological nature of the study, no formal sample size calculation was performed. Continuous variables are reported as median and interquartile range (IQR). Associations between baseline PEEPi,dyn and the physiological variables measured at T0 were

assessed using Spearman's rank correlation coefficient (ρ). Associations between baseline PEEPi,dyn and the changes in the considered variables were similarly explored using Spearman's rank correlation. Changes were expressed as percentage changes from baseline, except for TF,ic and TF,scm, for which absolute changes were used. Given the small sample size, uncertainty around Spearman's ρ was quantified using a non-parametric bootstrap: paired observations were resampled with replacement 100,000 times, and 95% confidence intervals (CIs) were derived from the 2.5th and 97.5th percentiles of the bootstrap distribution. No adjustment for multiple comparisons was performed. All analyses were performed with GraphPad Prism (GraphPad Software, San Diego, CA, USA) and IBM SPSS Statistics (IBM Corp., Armonk, NY, USA).

Use of Artificial Intelligence Tools

During the preparation of this thesis, the artificial intelligence–based platform OpenEvidence was used to support the preliminary bibliographic search and to assist with the rephrasing and linguistic revision of selected paragraphs. OpenEvidence was used only as an auxiliary tool and was not regarded as a substitute for the consultation of the original scientific literature. All information incorporated into the thesis was verified against the relevant original articles, guidelines, and other authoritative sources, which are cited directly. The author is solely responsible for the final wording, scientific accuracy, interpretation of the evidence, and conclusions presented in this thesis.

RESULTS

Patient population

Twelve patients with acute hypercapnic respiratory failure secondary to ECOPD completed the full physiological assessment described in the Methods; the screening and enrollment flow is shown in Figure 2, and individual clinical and gas-exchange data are reported in Figure 3.

With respect to background respiratory therapy, 8 patients were receiving single-inhaler triple therapy and 4 were on dual LAMA/LABA therapy, and 4 had received systemic corticosteroids within the preceding 6 months. Relevant comorbidities included chronic heart failure in 4 patients and diabetes mellitus in 6.

At baseline, patients presented with mild-to-moderate hypercapnic acidosis and moderately impaired oxygenation, with a median pH of 7.28, $PaCO_2$ of 66.3 mmHg, and PaO_2/FiO_2 of 150 mmHg. After 2 hours of standardized HFNC, gas exchange showed only a modest improvement, the median pH rising to 7.31, $PaCO_2$ falling to 64.6 mmHg, and PaO_2/FiO_2 increasing to 162 mmHg.

Figure 2. Study flowchart and assessment protocol.

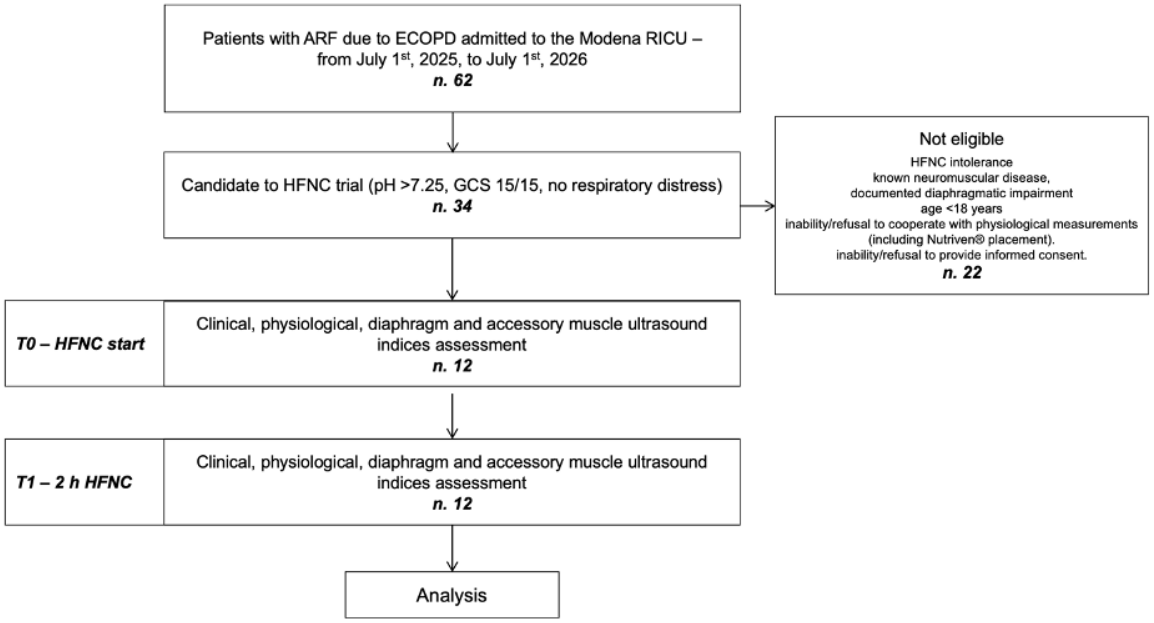


Figure 2. Flowchart illustrating patient screening, eligibility, enrolment, and study procedures. Clinical and physiological variables, together with diaphragm and accessory respiratory muscle ultrasound indices, were assessed at HFNC initiation (T0) and after 2 hours of HFNC treatment (T1). All 12 patients completed both assessments and were included in the analysis.

Abbreviations

ARF, acute respiratory failure; ECOPD, exacerbation of chronic obstructive pulmonary disease; GCS, Glasgow Coma Scale; HFNC, high-flow nasal cannula; RICU, Respiratory Intermediate Care Unit.

Figure 3. Individual clinical and gas-exchange characteristics at T0 and T1.

T0 – Baseline

N	GCS, value	MAP, mmHg	HR, bpm	pH	PaO_2/FiO_2, mmHg	PaO_2, mmHg	$PaCO_2$, mmHg	HCO_3^-, mmol/L	BE, mmol/L	Lac, mmol/L
1	15	80	87	7.28	135	74.4	61.6	28.2	2.3	0.6
2	15	83	65	7.25	151	60.2	69.6	29.1	3.2	1.0
3	15	123	95	7.29	259	72.6	54.1	25.4	0.6	1.2
4	15	97	87	7.28	79	55.0	66.2	30.3	4.0	2.1
5	15	84	73	7.34	130	52.1	69.6	36.6	10.5	1.0
6	15	110	100	7.31	195	68.3	56.1	27.0	1.2	0.3
7	15	83	89	7.25	158	63.0	77.5	32.9	5.8	1.0
8	15	117	117	7.31	201	60.4	53.9	26.2	0.4	0.8
9	15	83	83	7.26	148	59.3	71.5	31.0	4.2	1.4
10	15	98	98	7.28	188	65.7	66.5	30.2	3.7	1.0
11	15	100	100	7.27	143	71.3	74.1	32.9	6.1	1.0
12	15	87	87	7.31	142	56.7	54.3	26.4	0.6	1.1
Median, IQR	15 (15-15)	92 (83-103)	88 (84-99)	7.28 (7.27-7.31)	150 (137-193)	61.7 (57.5-70.6)	66.3 (54.8-71.3)	29.7 (26.9-31.5)	3.5 (1.1-4.6)	1.0 (0.9-1.2)

T1 – 2 hours after HFNC

N	GCS, value	MAP, mmHg	HR, bpm	pH	PaO_2/FiO_2, mmHg	PaO_2, mmHg	$PaCO_2$, mmHg	HCO_3^-, mmol/L	BE, mmol/L	Lac, mmol/L
1	15	93	87	7.24	120	72.1	64.2	26.5	-0.2	1.40
2	15	113	68	7.23	116	58.4	70.1	29.4	3.0	2.60
3	15	124	97	7.34	217	62.2	50.2	27.1	1.7	0.90
4	15	90	85	7.24	154	54.2	72.3	29.8	4.8	2.40
5	15	113	68	7.35	145	58.1	67.5	36.2	9.8	0.90
6	15	103	100	7.36	217	65.2	48.1	26.2	1.1	0.40
7	15	93	92	7.28	232	62.0	64.9	33.4	6.6	1.00
8	15	113	99	7.35	271	65.3	50.0	26.7	1.4	0.7
9	15	90	82	7.27	148	59.2	70.6	32.0	5.0	2.0
10	15	103	85	7.36	170	68.4	57.2	31.1	5.8	1.8
11	15	100	96	7.25	197	68.9	74.0	34.2	5.3	1.5
12	15	97	80	7.34	151	68.1	52.6	27.4	1.9	1.6
Median, IQR	15 (15-15)	102 (93-113)	86 (82-96)	7.31 (7.25-7.35)	162 (147-219)	65.0 (58.8-68.0)	64.6 (52.0-70.2)	29.6 (27.0-32.4)	3.9 (1.6-5.4)	1.5 (0.9-1.9)

Figure 3. Individual values are reported for each patient at T0, corresponding to baseline assessment at HFNC initiation, and at T1, corresponding to reassessment after 2 hours of HFNC treatment. Summary data are reported as median and interquartile range.

Abbreviations

BE, base excess; GCS, Glasgow Coma Scale; HCO_3^-, bicarbonate; HFNC, high-flow nasal cannula; HR, heart rate; IQR, interquartile range; Lac, lactate; MAP, mean arterial pressure; $PaCO_2$, arterial partial pressure of carbon dioxide; PaO_2, arterial partial pressure of oxygen.

Behaviour of physiological and clinical variables

Individual physiological measurements at both time points are reported in Figure 4 and Figure 5.

Dynamic intrinsic PEEP was measurable in every patient, confirming the presence of an inspiratory threshold load across the whole cohort, with a median PEEPi,dyn of 6.1 cmH_2O. Inspiratory effort was substantial and showed marked interindividual variability: median tidal Pes, Pdi, and Pnose swings were 15.2, 19.6, and 6.4 cmH_2O, respectively, and the corresponding time-integrated indices PTPes/min and PTPdi/min were 173 and 223 $cmH_2O \cdot s/min$. The median Pes/Pdi ratio was 0.70, and maximal diaphragmatic pressure-generating capacity (Pdi,sniff) was 46.1 cmH_2O, with a wide range across patients. Expiratory (abdominal) muscle activity was also detectable, the median Pga,rise being 1.7 cmH_2O.

Respiratory-muscle ultrasound indices reflected a distributed pattern of inspiratory-muscle activation, with median thickening fractions of 0.25 for the diaphragm (TF,di), 0.28 for the parasternal intercostals (TF,ic), and 0.11 for the sternocleidomastoids (TF,scm). The baseline breathing pattern was rapid and characterized by a short inspiratory time, with a median Ti of 0.69 s, Ti/Ttot of 0.32, and mean inspiratory flow (Vte/Ti) of 355 mL/s. Dyspnea was moderate to severe, with a median modified Borg score of 5.5.

After two hours of HFNC, the cohort as a whole showed only small median changes. Median PEEPi,dyn, tidal Pes, and Pnose swings were slightly reduced (to 5.7, 14.9, and 5.9 cmH_2O, respectively), and PTPes/min decreased modestly to 163 $cmH_2O \cdot s/min$, whereas PTPdi/min was essentially unchanged at 222 $cmH_2O \cdot s/min$. Median Pga,rise was comparable to baseline. The breathing pattern shifted toward a slower, deeper rhythm: Vte/PBW increased slightly, respiratory rate and the Borg dyspnea score decreased, inspiratory time lengthened (0.77 vs. 0.69 s), and mean inspiratory flow fell (305 mL/s), while Ti/Ttot was unchanged (0.33). Diaphragm thickening fraction remained substantially stable at the group level, whereas the intercostal and sternocleidomastoid thickening fractions increased after two hours of HFNC. Importantly, these median trends concealed considerable heterogeneity, which was more clearly captured by the correlations with baseline PEEPi,dyn described below.

Figure 4. Individual physiological characteristics at T0 and T1.

T0 – Baseline															
		Inspiratory effort		*Inspiratory effort partitioning and diaphragmatic mechanics*						*US-indices of respiratory muscles*				*Breathing pattern*	*Dyspnea*
N	**PEEPi,dyn, cmH$_2$O**	**Pes, cmH$_2$O**	**PTPes/min, cmH$_2$O*s/min**	**Pdi, cmH$_2$O**	**PTPdi/min, cmH$_2$O*s/min**	**Pdi, snif, cmH$_2$O**	**Pes/Pdi**	**Pnose, cmH$_2$O**	**Pga,rise cmH$_2$O**	**TF,di, ratio**	**TF, ic, ratio**	**TF,scm, ratio**	**TMax,di, ratio**	**Vte/PBW, mL/kg**	**RR, bpm**	**Borg, score**
1	8.7	18.2	185	26.2	271	31.3	0.69	8.7	2.7	0.15	0.30	0.11	0.88	3.7	32	7
2	7.3	20.8	227	19.4	209	21.3	1.07	9.2	2.9	0.17	0.40	0.19	0.91	2.8	28	6
3	4.2	7.5	89	14.4	171	81.2	0.52	3.6	0.5	0.41	0.00	0.05	0.66	5.8	22	5
4	5.9	19.9	246	23.6	271	26.4	0.84	8.9	3.7	0.14	0.80	0.35	1.00	3.3	29	6
5	4.1	8.6	125	13.5	168	77.2	0.64	3.6	0.4	0.27	0.00	0.06	0.83	6.1	25	3
6	3.4	10.2	138	14.3	180	89.2	0.71	2.6	0.7	0.29	0.00	0.00	0.62	5.9	24	4
7	3.2	9.8	135	16.4	215	77.2	0.60	2.0	1.1	0.38	0.05	0.00	0.63	4.4	23	2
8	3.8	8.9	121	14.4	164	85.2	0.62	3.1	0.6	0.34	0.00	0.00	0.63	6.4	23	5
9	7.5	16.2	201	19.8	231	41.5	0.82	6.7	1.7	0.29	0.31	0.13	0.75	3.5	27	4
10	7.0	18.1	198	21.7	244	38.0	0.83	6.7	1.9	0.14	0.29	0.17	0.80	3.4	29	6
11	6.8	16.6	177	23.5	262	49.0	0.70	7.1	1.6	0.17	0.32	0.18	0.75	3.9	31	6
12	6.2	14.2	169	20.8	231	43.2	0.68	6.0	2.0	0.24	0.26	0.12	0.90	4.6	28	6
Median, IQR	6.1 (4.0-7.1)	15.2 (9.6-18.1)	173 (133–199)	19.6 (14.4-22.2)	223 (178–249)	46.1 (36.3-78.2)	0.70 (0.63-0.82)	6.4 (3.5-7.5)	1.7 (0.7-2.2)	0.25 (0.16-0.30)	0.28 (0-0.31)	0.11 (0.04-0.18)	0.78 (0.65-0.89)	4.1 (3.5-5.9)	28 (24-29)	5.5 (4-6)

T1 – 2 hours after HFNC															
		Inspiratory effort		*Inspiratory effort partitioning and diaphragmatic mechanics*						*US-indices of respiratory muscles*				*Breathing pattern*	*Dyspnea*
N	**PEEPi,dyn, cmH_2O**	**Pes, cmH_2O**	**PTPes/min, cmH_2O*s/min**	**Pdi, cmH_2O**	**PTPdi/min, cmH_2O*s/min**	**Pdi,snif, cmH_2O**	**Pes/Pdi**	**Pnose, cmH_2O**	**Pga,rise cmH_2O**	**TF,di, ratio**	**TF,ic, ratio**	**TF,scm, ratio**	**TMax,di, ratio**	**Vte/PBW, mL/kg**	**RR, bpm**	**Borg, score**
1	8.5	18.7	210	24.0	268	28.3	0.78	9.4	2.5	0.10	0.39	0.18	0.88	3.6	29	6
2	8.1	23.2	271	17.8	210	21.4	1.30	10.5	3.9	0.11	0.70	0.25	0.95	2.6	26	6
3	4.0	6.5	75	16.0	185	81.2	0.41	2.8	0.5	0.41	0.00	0.00	0.66	6.0	23	3
4	6.5	21.2	250	20.0	237	24.3	1.06	10.2	3.0	0.14	0.90	0.45	1.00	3.0	26	6
5	3.2	8.0	102	17.0	180	81.2	0.47	3.2	0.4	0.33	0.00	0.06	0.70	6.7	16	3
6	2.1	7.2	90	12.0	149	89.4	0.60	1.8	0.6	0.39	0.00	0.00	0.60	6.4	20	3
7	2.2	9.0	115	21.2	269	92.3	0.42	1.8	0.3	0.44	0.00	0.00	0.59	5.5	18	2
8	2.5	6.0	85	14.0	139	85.3	0.43	2.3	0.3	0.41	0.00	0.00	0.63	6.7	16	2
9	5.6	18.2	216	20.0	237	38.0	0.91	6.8	1.5	0.29	0.38	0.23	0.71	3.7	25	3
10	6.0	15.3	178	19.1	225	37.2	0.80	5.7	2.3	0.14	0.47	0.26	0.77	3.4	26	5
11	5.8	15.4	162	20.9	219	47.1	0.74	7.0	1.6	0.22	0.41	0.25	0.74	3.9	28	6
12	6.5	14.5	164	23.1	261	42.9	0.63	6.1	2.3	0.24	0.37	0.20	0.93	4.6	28	5
Median, IQR	5.7 (3.5-6.5)	14.9 (7.8-18.3)	163 (99–212)	19.6 (16.8-21.0)	222 (183–249)	45.0 (35.0-82.2)	0.68 (0.46-0.83)	5.9 (2.3-8.8)	1.6 (0.5-2.4)	0.26 (0.14-0.39)	0.38 (0-0.42)	0.19 (0-0.25)	0.72 (0.65-0.89)	4.3 (3.5-6.1)	26 (20-27)	5 (3-6)

Figure 4. Individual values are reported for each patient at T0, corresponding to baseline assessment at HFNC initiation, and at T1, corresponding to reassessment after two hours of HFNC treatment. Summary data are presented as median and interquartile range (IQR).

Variables are grouped as inspiratory effort, inspiratory effort partitioning and diaphragmatic mechanics, ultrasound (US) indices of the respiratory muscles, breathing pattern, and dyspnea

Abbreviations

Borg, modified Borg dyspnea score; HFNC, high-flow nasal cannula; Pdi, tidal transdiaphragmatic pressure swing; Pdi,sniff, maximal transdiaphragmatic pressure during sniff manoeuvre; PEEPi,dyn, dynamic intrinsic positive end-expiratory pressure (corrected for the abdominal contribution, i.e. uncorrected PEEPi,dyn minus Pga,decay); Pes, tidal inspiratory esophageal pressure swing; Pes/Pdi, ratio of tidal esophageal to transdiaphragmatic pressure swing; Pga,rise, expiratory gastric pressure rise; Pnose, tidal nasal pressure swing; PTPdi/min, transdiaphragmatic pressure–time product per minute; PTPes/min, esophageal pressure–time product per minute; RR, respiratory rate; TF,di, diaphragm thickening fraction; TF,ic, parasternal intercostal thickening fraction; TF,scm, sternocleidomastoid thickening fraction; TMax,di, diaphragmatic recruitment index during maximal sniff; Vte/PBW, expiratory tidal volume normalized to predicted body weight.

Figure 5. Individual breathing pattern, respiratory timing, and per-breath pressure–time products at T0 and T1.

T0 – Baseline						
N	**Ti/Ttot**	**Ti (s)**	**Vte/Ti (ml/s)**	**Vte (ml)**	**PTPes/breath ($cmH_2O \cdot s$)**	**PTPdi/breath ($cmH_2O \cdot s$)**
1	0.29	0.54	330	180	5.4	8.4
2	0.31	0.66	250	167	8.1	7.5
3	0.35	0.95	410	385	4.1	7.9
4	0.31	0.65	310	202	8.2	9.2
5	0.34	0.81	440	354	4.5	6.7
6	0.34	0.86	470	403	5.5	7.6
7	0.35	0.91	360	323	5.6	9.1
8	0.35	0.90	440	394	4.9	7.9
9	0.31	0.70	330	231	6.8	8.3
10	0.31	0.64	350	223	7.2	8.5
11	0.30	0.58	450	262	5.9	8.4
12	0.32	0.68	350	237	6.0	8.6
Median, IQR	0.32 (0.31–0.35)	0.69 (0.65–0.87)	355 (330–440)	250 (218-361)	5.8 (5.3–6.9)	8.4 (7.8–8.5)

T1 – 2 hours after HFNC						
N	**Ti/Ttot**	**Ti (s)**	**Vte/Ti (ml/s)**	**Vte (ml)**	**PTPes/breath ($cmH_2O \cdot s$)**	**PTPdi/breath ($cmH_2O \cdot s$)**
1	0.30	0.62	280	174	7.2	9.1
2	0.31	0.72	210	155	10.3	7.9
3	0.34	0.90	440	395	3.2	8.0
4	0.32	0.74	250	186	9.5	9.1
5	0.37	1.39	280	388	6.1	10.2
6	0.36	1.09	400	433	4.4	7.5
7	0.37	1.23	330	402	6.8	13.7
8	0.37	1.39	300	414	5.4	8.7
9	0.33	0.79	310	247	8.3	9.5
10	0.32	0.75	300	223	7.1	8.6
11	0.32	0.68	390	263	6.5	8.2
12	0.31	0.67	360	241	6.1	9.3
Median, IQR	0.33 (0.32–0.37)	0.77 (0.71–1.13)	305 (280–370)	255 (214-397)	6.7 (5.9–7.5)	8.9 (8.2–9.4)

Figure 5. Individual values are reported for each patient at T0, corresponding to baseline assessment at HFNC initiation, and at T1, corresponding to reassessment after 2 hours of HFNC treatment. Summary data are reported as median and interquartile range (IQR).

Abbreviations

HFNC, high-flow nasal cannula; PTPdi/breath, transdiaphragmatic pressure–time product per breath; PTPes/breath, esophageal pressure–time product per breath; Ti, inspiratory time; Ti/Ttot, duty cycle (inspiratory time/total breath duration); Vte, absolute expiratory tidal volume; Vte/Ti, mean inspiratory flow.

Baseline PEEPi,dyn and the cross-sectional physiological profile

Inspiratory effort. The association between baseline PEEPi,dyn and the magnitude of inspiratory effort is shown in Figure 6. Higher PEEPi,dyn was directly correlated with both tidal Pes (ρ=0.69, panel A) and PTPes/min (ρ=0.68, panel B), indicating that patients with a larger inspiratory threshold load generated greater instantaneous and time-integrated inspiratory effort.

Figure 6. Association between dynamic intrinsic PEEP and inspiratory effort at baseline

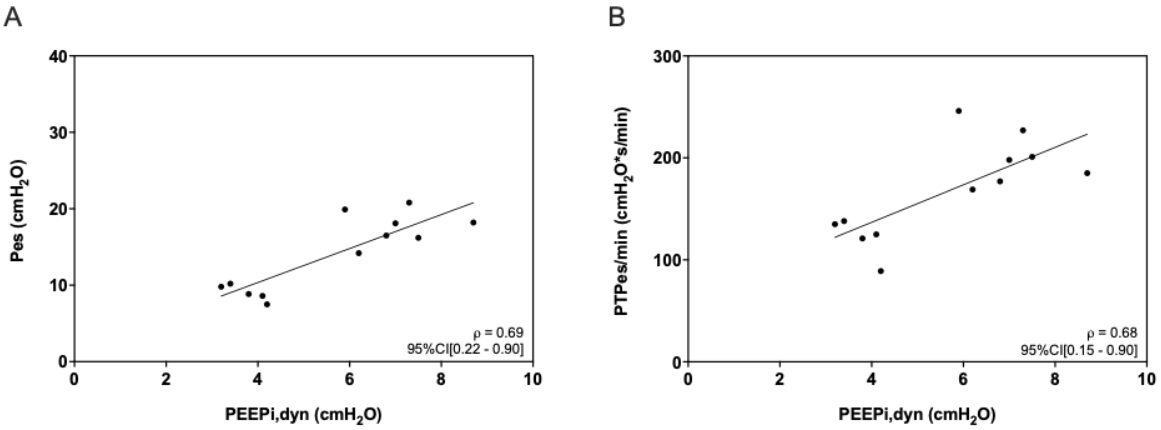


Figure 6. Scatterplots showing the association between baseline dynamic intrinsic positive end-expiratory pressure (PEEPi,dyn) and esophageal pressure swing (Pes; panel A) and esophageal pressure–time product per minute (PTPes; panel B). Solid lines represent linear regression fits. Spearman's correlation coefficients (ρ) and corresponding 95% confidence intervals are reported in each panel.

Abbreviations

CI, confidence interval; PEEPi,dyn, dynamic intrinsic positive end-expiratory pressure; Pes, esophageal pressure swing; PTPes/min, esophageal pressure–time product per minute.

Effort partitioning and diaphragmatic mechanics. The corresponding associations are shown in Figure 7. PEEPi,dyn was directly correlated with tidal Pdi (ρ=0.69, panel A), PTPdi/min (ρ=0.60, panel B), and the nasal pressure swing Pnose (ρ=0.82, panel C), the latter confirming that this non-invasive index tracked the increase in inspiratory effort. In contrast, maximal diaphragmatic pressure-generating capacity was inversely related to PEEPi,dyn (Pdi,sniff; ρ=−0.77, panel D), indicating that a greater threshold load coexisted with a lower diaphragmatic reserve. Expiratory muscle activity increased in parallel, PEEPi,dyn being directly correlated with Pga,rise (ρ=0.64, panel E), whereas no clear association was observed for the Pes/Pdi ratio (panel F).

Figure 7. Association between dynamic intrinsic PEEP and inspiratory effort partitioning and diaphragmatic mechanics at baseline

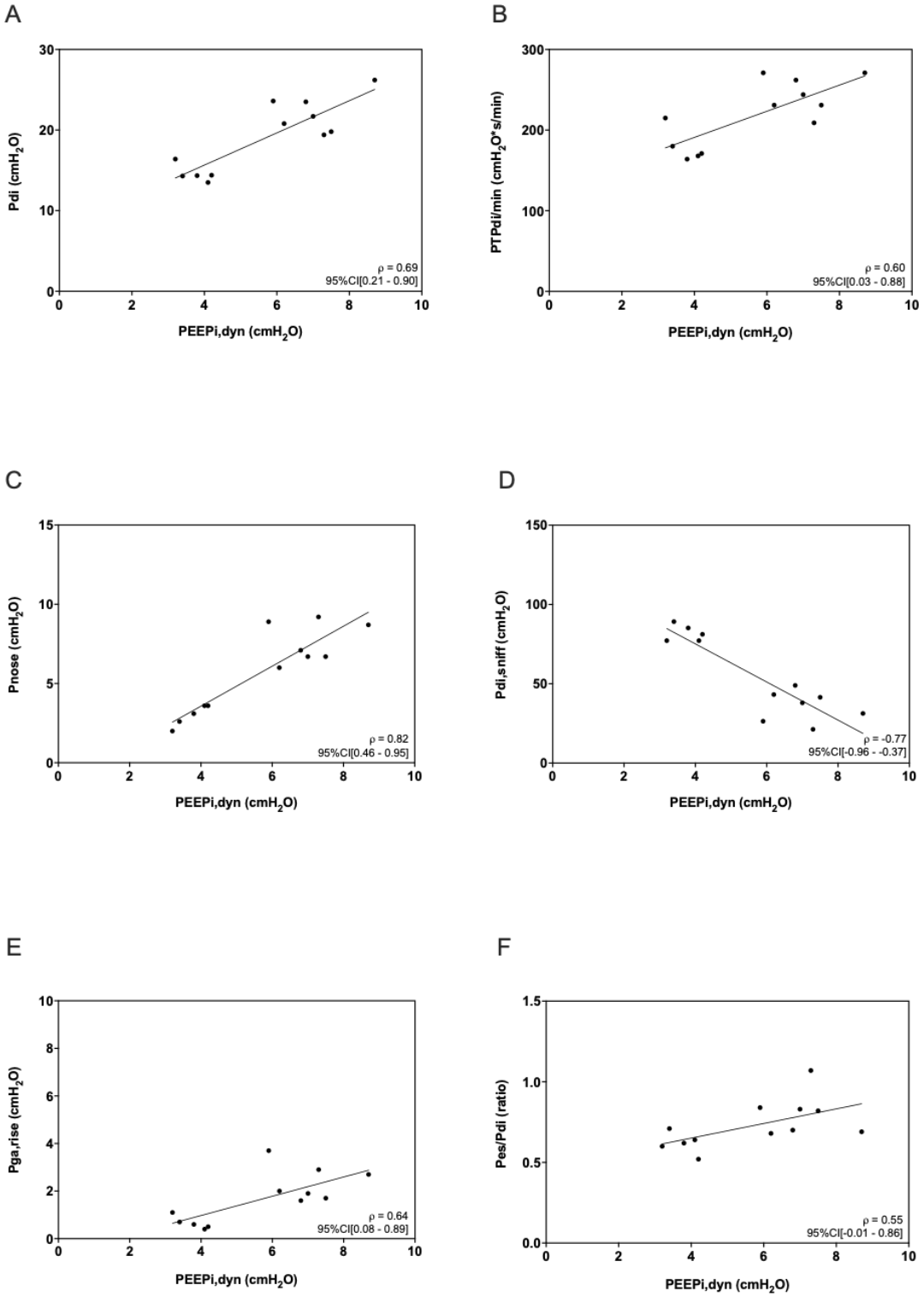


Figure 7. Scatterplots showing the association between baseline dynamic intrinsic positive end-expiratory pressure (PEEPi,dyn) and transdiaphragmatic pressure swing (Pdi; panel A), transdiaphragmatic pressure-time product per minute (PTPdi/min; panel B), nasal pressure

swing (Pnose; panel C), sniff transdiaphragmatic pressure (Pdi,sniff; panel D), expiratory gastric pressure rise (Pga,rise; panel E), and the ratio of esophageal to transdiaphragmatic pressure swings (Pes/Pdi; panel F). Solid lines represent linear regression fits. Spearman's correlation coefficients (ρ) and corresponding 95% confidence intervals are reported in each panel.

Abbreviations

CI, confidence interval; Pdi, transdiaphragmatic pressure swing; Pdi,sniff, sniff transdiaphragmatic pressure; PEEPi,dyn, dynamic intrinsic positive end-expiratory pressure; Pes, esophageal pressure swing; Pga,rise, expiratory gastric pressure rise; Pnose, nasal pressure swing; PTPdi/min, transdiaphragmatic pressure-time product per minute.

Respiratory-muscle ultrasound and breathing pattern. These associations are presented in Figure 8. Higher PEEPi,dyn was inversely correlated with diaphragm thickening fraction (TF,di; $\rho=-0.60$, panel A) and directly correlated with intercostal (TF,ic; $\rho=0.68$, panel B) and sternocleidomastoid (TF,scm; $\rho=0.72$, panel C) thickening fractions, consistent with a redistribution of inspiratory activity from the diaphragm toward the extra-diaphragmatic and accessory muscles as the threshold load increased. The diaphragmatic recruitment index during maximal sniff (TMax,di) tended to rise with PEEPi,dyn, but this association was less clear ($\rho=0.59$, panel D). At the same time, higher PEEPi,dyn was associated with a lower mean inspiratory flow (Vte/Ti; $\rho=-0.64$, panel E) and a higher respiratory rate ($\rho=0.71$, panel F).

Figure 8. Association between dynamic intrinsic PEEP, respiratory muscle ultrasound indices, and breathing pattern at baseline

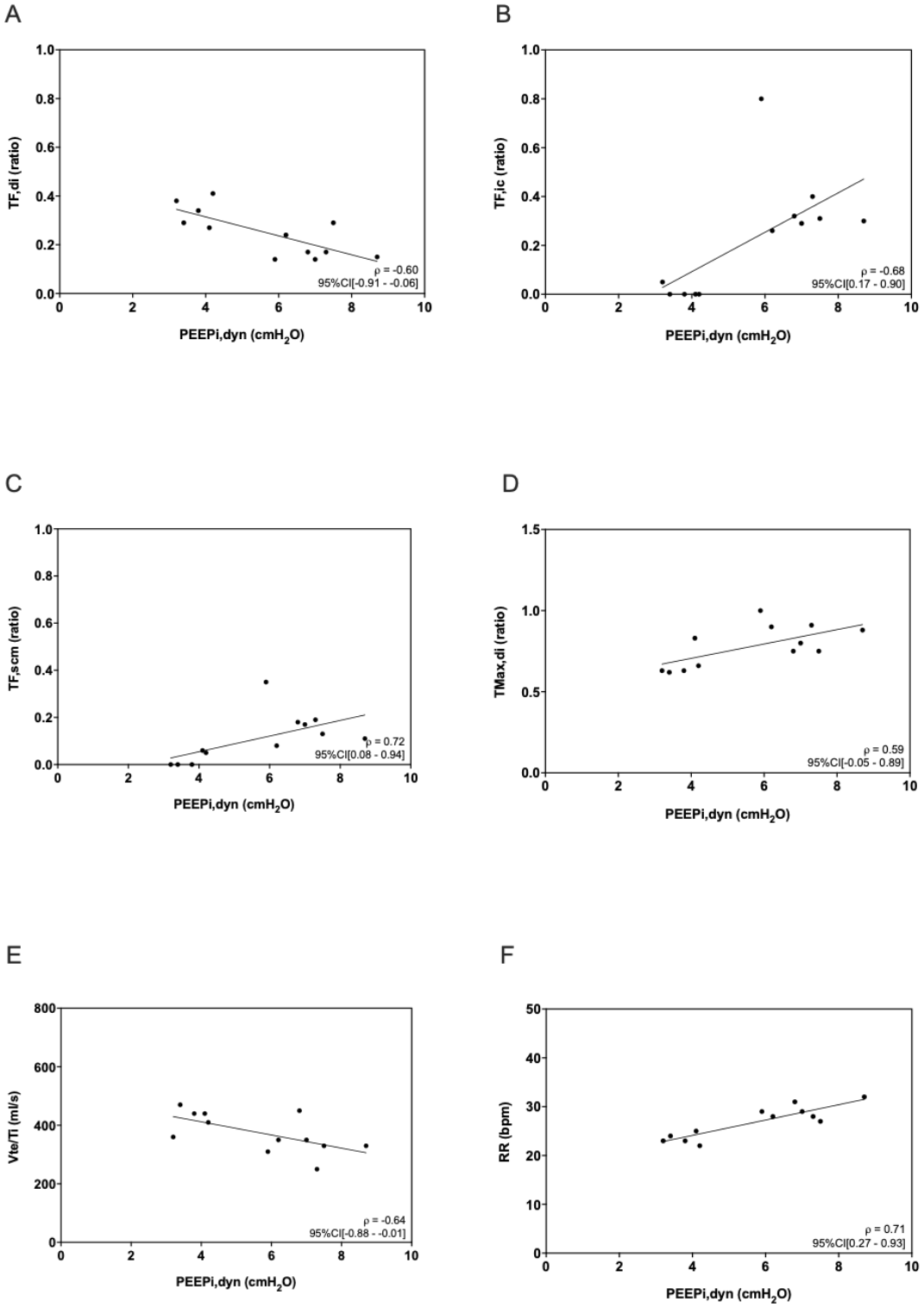


Figure 8. Scatterplots showing the association between baseline dynamic intrinsic positive end-expiratory pressure (PEEPi,dyn) and diaphragmatic thickening fraction (TF,di; panel A), intercostal muscle thickening fraction (TF,ic; panel B), sternocleidomastoid muscle thickening

fraction (TF,scm; panel C), diaphragmatic recruitment index during maximal sniff (TMax,di; panel D), mean inspiratory flow (Vte/Ti; panel E), and respiratory rate (RR; panel F). Solid lines represent linear regression fits. Spearman's correlation coefficients (ρ) and corresponding 95% confidence intervals are reported in each panel.

Abbreviations

CI, confidence interval; PEEPi,dyn, dynamic intrinsic positive end-expiratory pressure; RR, respiratory rate; TF,di, diaphragmatic thickening fraction; TF,ic, intercostal muscle thickening fraction; TF,scm, sternocleidomastoid muscle thickening fraction; Ti, inspiratory time; TMax,di, diaphragmatic recruitment index during maximal sniff; Vte, expiratory tidal volume; Vte/Ti, mean inspiratory flow.

Additional breathing-pattern and effort indices, and dyspnea. These are reported in Figure 9. PEEPi,dyn was inversely correlated with expiratory tidal volume, both in absolute terms (Vte; $\rho=-0.80$, panel A) and normalized to predicted body weight (Vte/PBW; $\rho=-0.69$, panel B), and with the duty cycle (Ti/Ttot; $\rho=-0.87$, panel C), indicating that a greater threshold load was associated with a lower and less efficient tidal ventilation. No clear associations were observed with the per-breath pressure–time products (PTPes/breath, $\rho=0.43$, panel D; PTPdi/breath, $\rho=0.06$, panel E), suggesting that the effort–load relationship was driven mainly by the minute-integrated rather than the per-breath indices. Finally, the Borg dyspnea score was directly correlated with PEEPi,dyn ($\rho=0.61$, panel F), linking the mechanical burden to the symptom experienced by the patient.

Figure 9. Association between dynamic intrinsic PEEP, additional breathing-pattern indices, dyspnea, and inspiratory effort per breath at baseline.

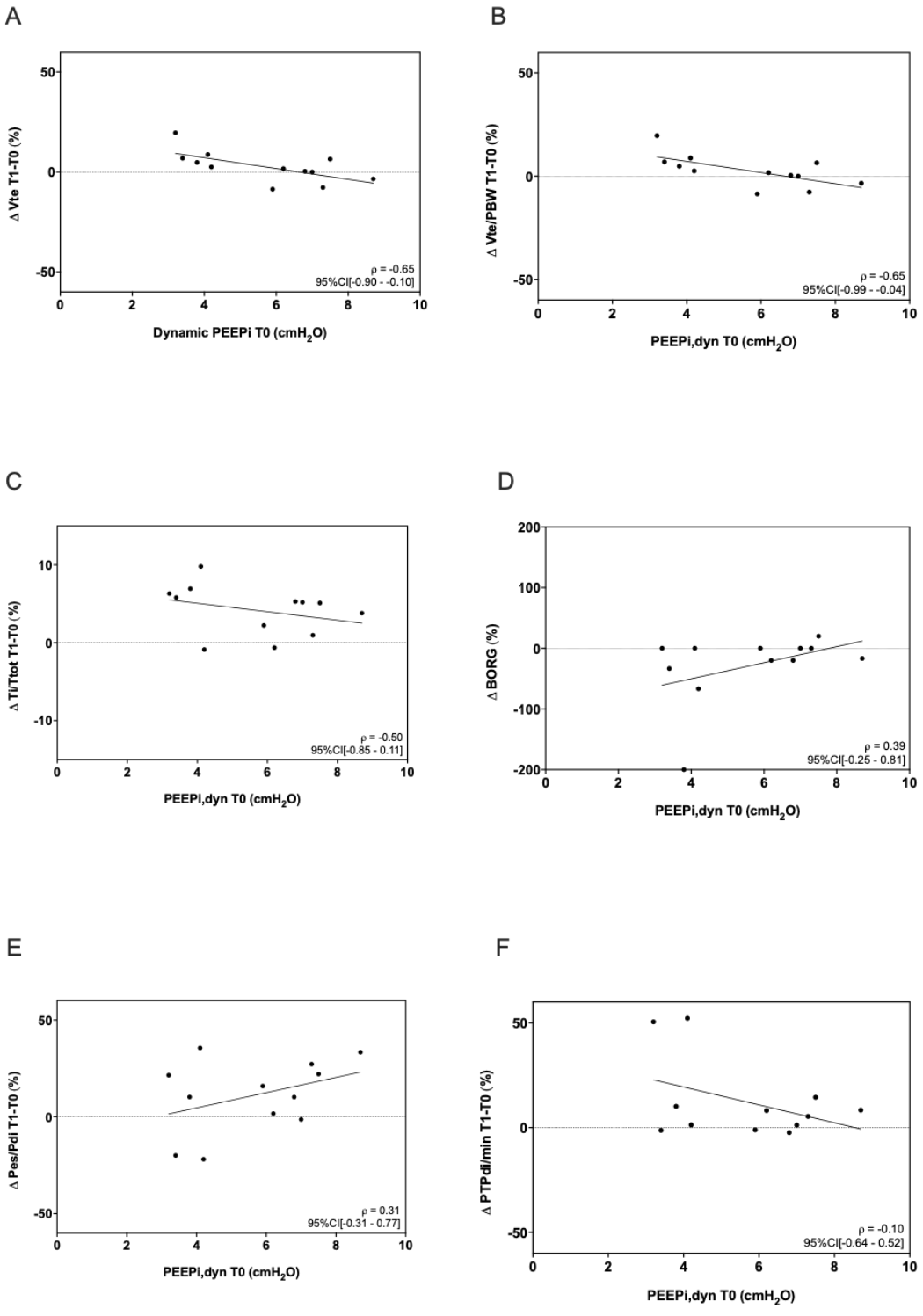


Figure 9. Scatter plots showing the association between dynamic intrinsic positive end-expiratory pressure (PEEPi,dyn) measured at baseline (T0) and expiratory tidal volume (Vte; panel A), expiratory tidal volume normalized to predicted body weight (Vte/PBW; panel B),

inspiratory duty cycle (Ti/Ttot; panel C), esophageal pressure–time product per breath (PTPes/breath; panel D), transdiaphragmatic pressure–time product per breath (PTPdi/breath; panel E), and Borg dyspnea score (panel F).

Abbreviations

CI, confidence interval; PBW, predicted body weight; PEEPi,dyn, dynamic intrinsic positive end-expiratory pressure; PTPdi/breath, transdiaphragmatic pressure–time product per breath; PTPes/breath, esophageal pressure–time product per breath; Ti, inspiratory time; Ttot, total respiratory cycle time; Vte, expiratory tidal volume.

Baseline PEEPi,dyn and the early physiological response to HFNC

Inspiratory effort and diaphragmatic mechanics. The associations between baseline PEEPi,dyn and the T0–T1 changes in effort-related variables are shown in Figure 10. Higher baseline PEEPi,dyn was directly correlated with the percentage changes in tidal Pes (ρ=0.69, panel A) and PTPes/min (ρ=0.84, panel B) and with the percentage change in Pnose (ρ=0.61, panel C), indicating that patients with the largest baseline threshold load tended to show persistence or worsening of inspiratory effort rather than unloading during HFNC. In the same direction, higher baseline PEEPi,dyn was associated with a greater increase in the Pes/Pdi ratio (ρ=0.77, panel E) and a greater reduction in Pdi,sniff (ρ=−0.72, panel D), consistent with a shift toward extra-diaphragmatic effort and a decline in diaphragmatic reserve, whereas no clear association was observed with the percentage change in PTPdi/min (panel F).

Figure 10. Association between baseline dynamic intrinsic positive end-expiratory pressure and changes in inspiratory effort and diaphragmatic mechanics during HFNC

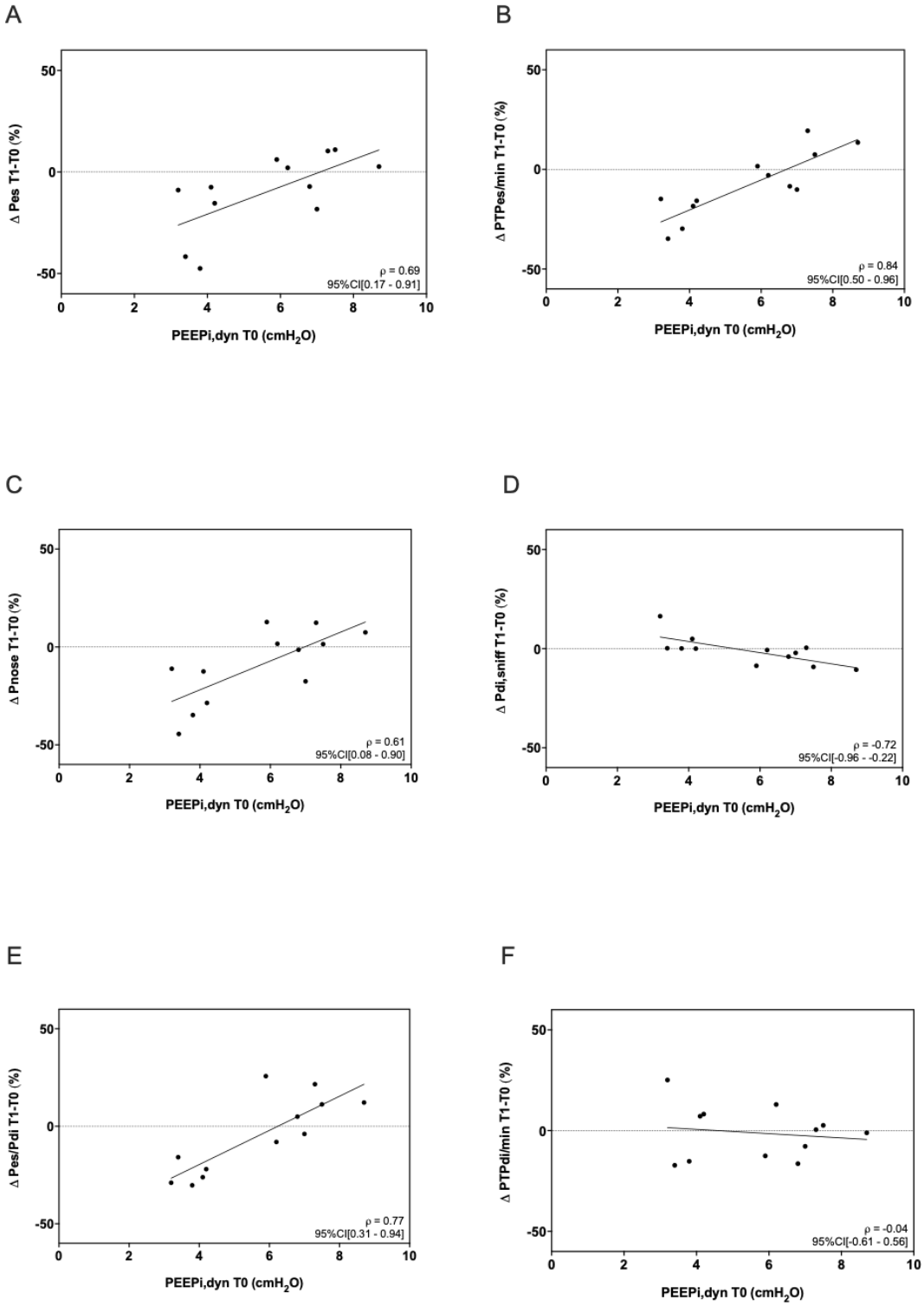


Figure 10. Scatter plots showing the association between dynamic intrinsic positive end-expiratory pressure (PEEPi,dyn) measured at baseline (T0) and percentage changes from T0 to T1 in tidal esophageal pressure swing (Pes; **panel A**), esophageal pressure–time product per

minute (PTPes/min; **panel B**), nasal pressure swing (Pnose; **panel C**), maximal transdiaphragmatic pressure during sniff (Pdi,sniff; **panel D**), Pes/Pdi ratio (**panel E**), and transdiaphragmatic pressure–time product per minute (PTPdi/min; **panel F**). Solid lines represent linear regression fits. Spearman's correlation coefficients (ρ) and corresponding 95% confidence intervals (CI) are reported within each panel.

Abbreviations

CI, confidence interval; HFNC, high-flow nasal cannula; Pdi, tidal transdiaphragmatic pressure swing; Pdi,sniff, maximal transdiaphragmatic pressure during sniff; PEEPi,dyn, dynamic intrinsic positive end-expiratory pressure; Pes, tidal esophageal pressure swing; Pnose, nasal pressure swing; PTPdi/min, transdiaphragmatic pressure–time product per minute; PTPes/min, esophageal pressure–time product per minute; T0, baseline assessment at HFNC initiation; T1, assessment after 2 hours of HFNC.

Respiratory-muscle recruitment and breathing pattern. Figure 11 illustrates these associations. Higher baseline PEEPi,dyn was inversely correlated with the percentage change in diaphragm thickening fraction (TF,di; $\rho=-0.72$, panel A) and directly correlated with the absolute changes in intercostal (TF,ic; $\rho=0.73$, panel B) and sternocleidomastoid (TF,scm; $\rho=0.63$, panel C) thickening fractions, as well as with the percentage change in TMax,di ($\rho=0.74$, panel D). Taken together, these findings indicate a progressive redistribution of inspiratory activity away from the diaphragm and toward the accessory muscles in patients with greater baseline dynamic hyperinflation. No clear associations were observed with the percentage change in mean inspiratory flow (Vte/Ti; $\rho=0.11$, panel E) or respiratory rate ($\rho=0.59$, panel F).

Figure 11. Association between baseline dynamic intrinsic positive end-expiratory pressure and changes in respiratory muscle ultrasound indices and breathing pattern during HFNC.

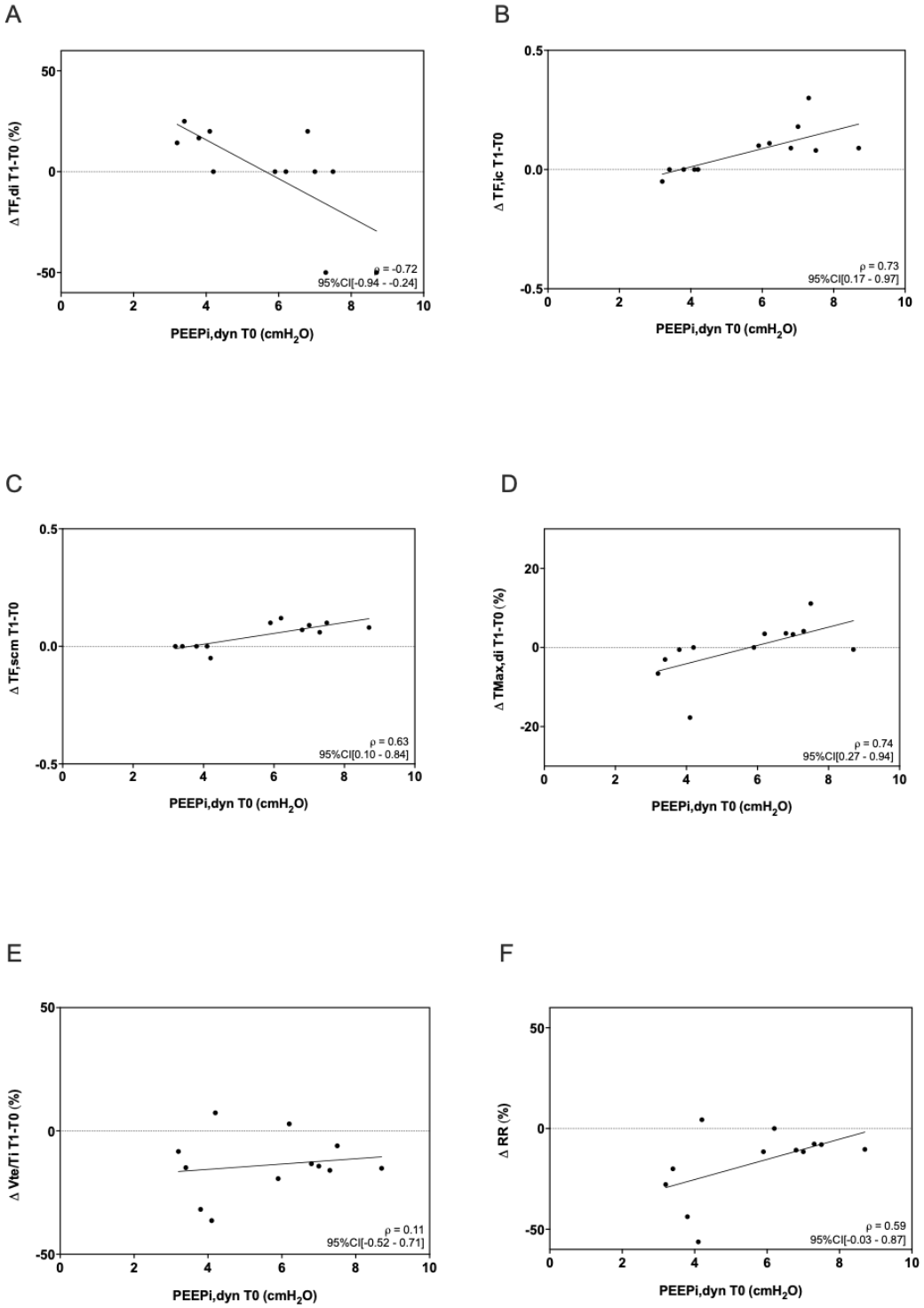


Figure 11. Scatter plots showing the association between dynamic intrinsic positive end-expiratory pressure (PEEPi,dyn) measured at baseline (T0) and changes from T0 to T1 in respiratory muscle ultrasound indices and breathing pattern: percentage change in diaphragm

thickening fraction (TF,di; **panel A**), absolute change in parasternal intercostal thickening fraction (TF,ic; **panel B**), absolute change in sternocleidomastoid thickening fraction (TF,scm; **panel C**), percentage change in diaphragmatic recruitment index during maximal sniff (TMax,di; **panel D**), percentage change in mean inspiratory flow (Vte/Ti; **panel E**), and percentage change in respiratory rate (RR; **panel F**). Solid lines represent linear regression fits. Spearman's correlation coefficients (ρ) and corresponding 95% confidence intervals (CI) are reported within each panel.

Abbreviations

CI, confidence interval; HFNC, high-flow nasal cannula; PEEPi,dyn, dynamic intrinsic positive end-expiratory pressure; RR, respiratory rate; TF,di, diaphragm thickening fraction; TF,ic, parasternal intercostal thickening fraction; TF,scm, sternocleidomastoid thickening fraction; TMax,di, diaphragmatic recruitment index during maximal sniff; T0, baseline assessment at HFNC initiation; T1, assessment after 2 hours of HFNC; Ti, inspiratory time; Vte, expiratory tidal volume; Vte/Ti, mean inspiratory flow.

Further longitudinal associations. Additional associations are reported in Figure 12 and Figure 13. Higher baseline PEEPi,dyn was associated with persistence or worsening of PEEPi,dyn during HFNC (ρ=0.76) and with less favourable changes in Vte and Vte/PBW (ρ=−0.65 for both), whereas no clear associations were observed with the changes in tidal Pdi, Borg dyspnea score, Pga,rise, Ti/Ttot, or the per-breath pressure–time products.

Figure 12. Association between baseline dynamic intrinsic positive end-expiratory pressure and additional changes in respiratory mechanics during HFNC.

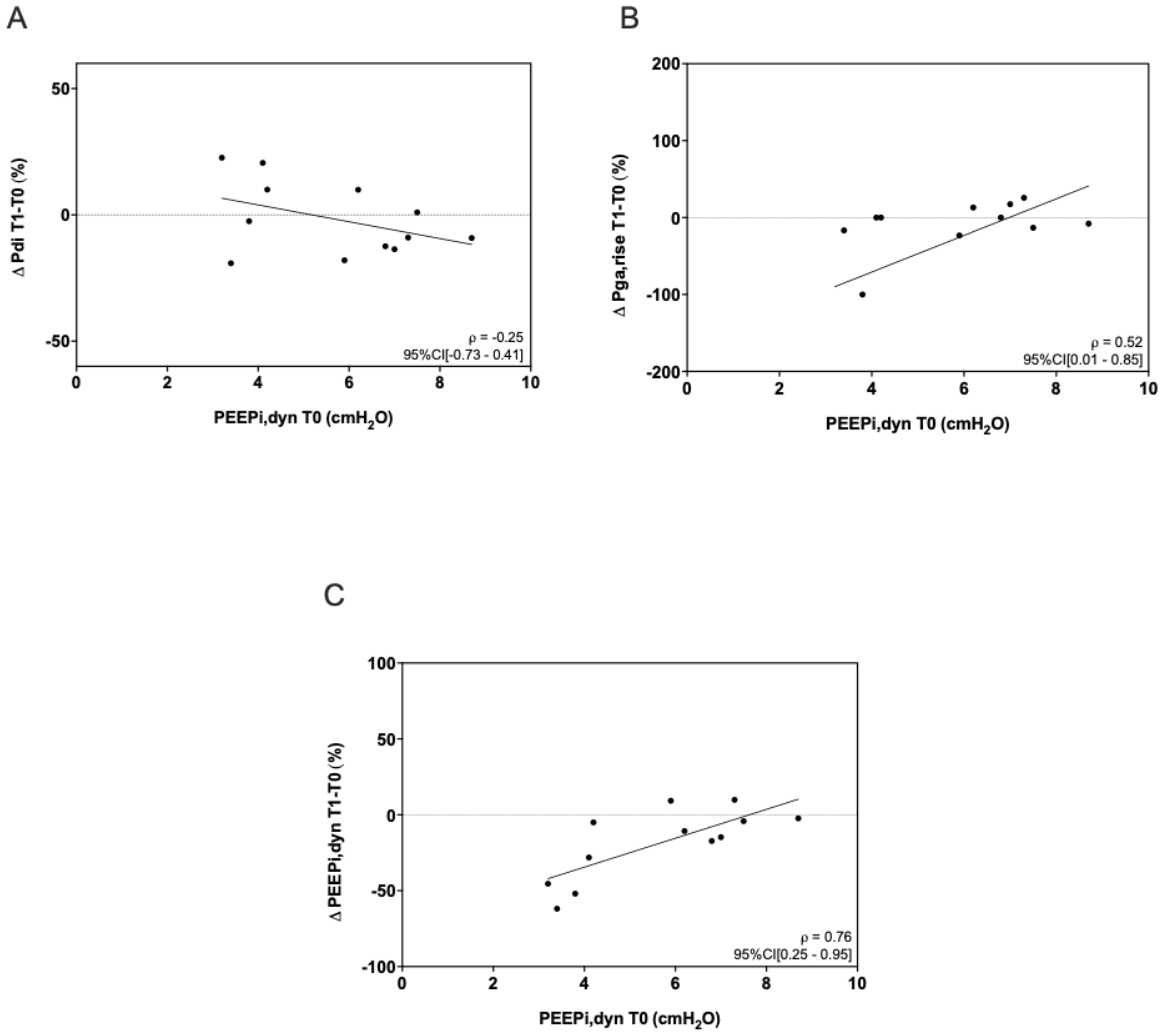


Figure 12. Scatter plots showing the association between dynamic intrinsic positive end-expiratory pressure (PEEPi,dyn) measured at baseline (T0) and percentage changes from T0 to T1 in tidal transdiaphragmatic pressure swing (Pdi; panel A), gastric pressure rise during

expiration (Pga,rise; panel B), and PEEPi,dyn (panel C). Solid lines represent linear regression fits. Spearman's correlation coefficients (ρ) and corresponding 95% confidence intervals (CI) are reported within each panel.

Abbreviations

CI, confidence interval; HFNC, high-flow nasal cannula; Pdi, tidal transdiaphragmatic pressure swing; PEEPi,dyn, dynamic intrinsic positive end-expiratory pressure; Pga,rise, gastric pressure rise during expiration; T0, baseline assessment at HFNC initiation; T1, assessment after 2 hours of HFNC

Figure 13. Association between baseline dynamic intrinsic positive end-expiratory pressure and additional breathing pattern, ventilatory, and inspiratory effort variables

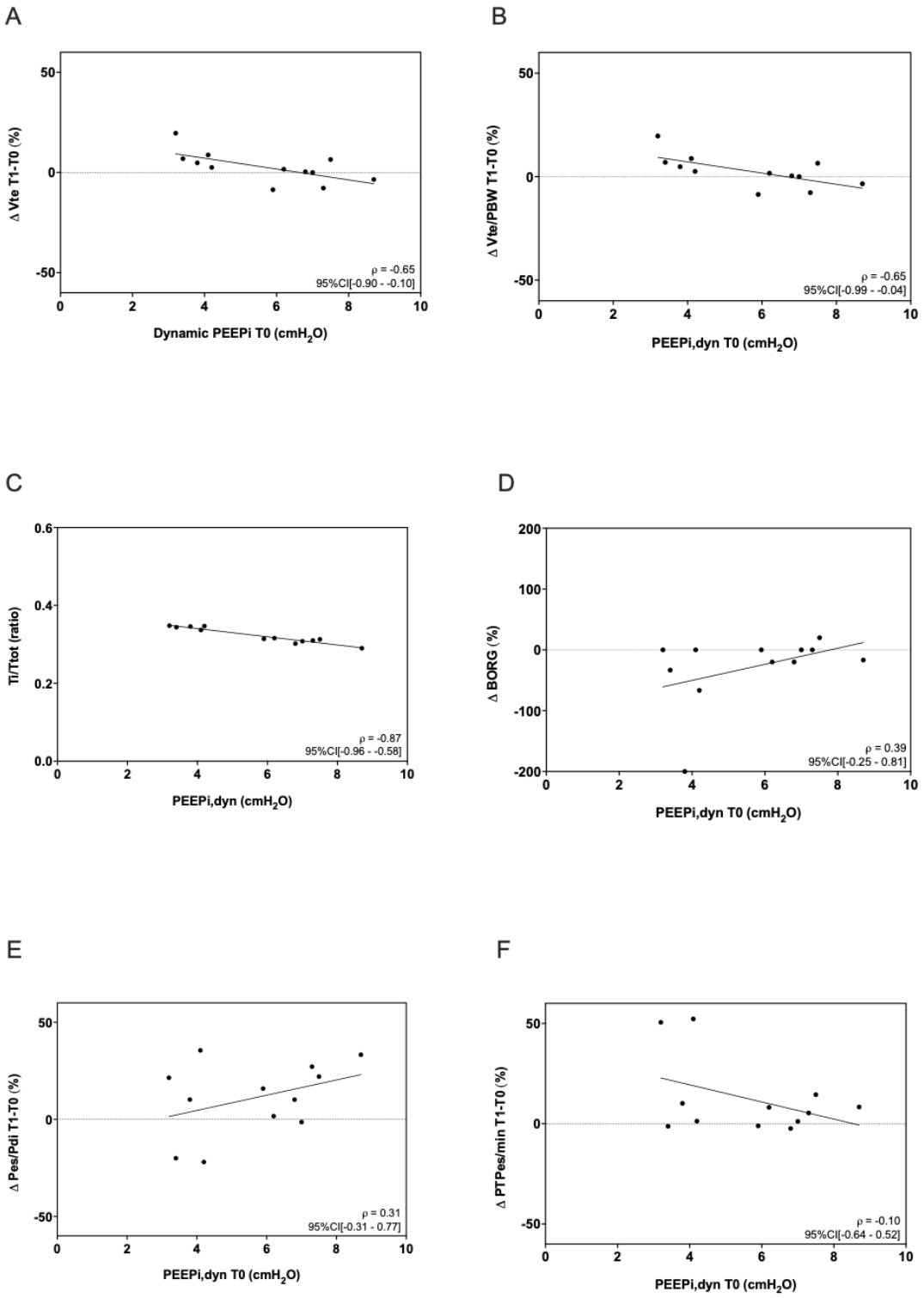


Figure 13. Scatter plots showing the association between dynamic intrinsic positive end-expiratory pressure (PEEPi,dyn) measured at baseline (T0) and percentage changes from T0 to T1 in expiratory tidal volume (Vte; panel A) and expiratory tidal volume normalized to

predicted body weight (Vte/PBW; panel B), inspiratory duty cycle (Ti/Ttot; panel C), and Borg dyspnea score (panel D), Pes/Pdi ratio (panel E), and esophageal pressure–time product per minute (PTPes/min; panel F). Solid lines represent linear regression fits. Spearman's correlation coefficients (ρ) and corresponding 95% confidence intervals (CI) are reported within each panel.

Abbreviations

Borg, Borg dyspnea score; CI, confidence interval; Pdi, tidal transdiaphragmatic pressure swing; PEEPi,dyn, dynamic intrinsic positive end-expiratory pressure; Pes, tidal esophageal pressure swing; PTPes/min, esophageal pressure–time product per minute; PBW, predicted body weight; T0, baseline assessment at HFNC initiation; T1, assessment after two hours of HFNC; Ti, inspiratory time; Ttot, total respiratory cycle time; Vte, expiratory tidal volume.

DISCUSSION

In this prospective physiological study of spontaneously breathing patients with ECOPD supported with HFNC, a higher baseline dynamic intrinsic PEEP (PEEPi,dyn) was consistently associated with a more adverse respiratory phenotype: greater inspiratory effort, impaired diaphragmatic mechanics, a shift of inspiratory activity toward the extra-diaphragmatic and accessory muscles, a less efficient breathing pattern, and more intense dyspnea. The same baseline threshold load was also associated with a less favourable physiological trajectory over the first two hours of HFNC, characterized by persistence or worsening of inspiratory effort, progressive extra-diaphragmatic recruitment, and persistence or worsening of PEEPi,dyn itself, indicating incomplete respiratory unloading. To our knowledge, this is the first study to connect PEEPi,dyn to both the cross-sectional mechanical burden and the early dynamic response to HFNC in spontaneously breathing patients during an acute exacerbation, a setting in which the interaction between threshold load, effort partitioning, and a specific non-invasive support is most clinically relevant.

PEEPi,dyn as an inspiratory threshold load. The association between PEEPi,dyn and the magnitude of inspiratory effort is physiologically coherent and reproduces, in the acute spontaneously breathing patient, a mechanism previously characterized mainly in mechanically ventilated or stable patients. Because expiratory flow limitation and loss of elastic recoil prolong the expiratory time constant, expiration remains incomplete and alveolar pressure stays positive at end-expiration; before inspiratory flow can begin, the inspiratory muscles must first generate an equal and opposite negative pressure to bring alveolar pressure below atmospheric level (19). This fraction of muscular pressure is dissipated against the threshold load without contributing to tidal ventilation, so that a substantial share of each contraction is mechanically "wasted" (19,21). In our cohort this was directly reflected by the graded increase in tidal Pes, PTPes/min, Pdi, and Pnose swings with increasing PEEPi,dyn, confirming that patients with the largest threshold load generated the greatest instantaneous and time-integrated effort. The parallel increase in expiratory gastric pressure rise (Pga,rise) indicates that greater loading was accompanied by active recruitment of the expiratory (abdominal) muscles (23). This is mechanistically important, because expiratory muscle contraction can raise intrinsic PEEP independently of the degree of dynamic hyperinflation and can further compress the flow-limited airways, aggravating gas trapping (23). These cross-sectional associations therefore should not be read as a simple unidirectional cause-and-effect relationship: PEEPi,dyn increases the inspiratory threshold load, but the resulting expiratory muscle activity may in turn

feed back to increase PEEPi,dyn, consistent with the self-reinforcing mechanical cycle that characterizes ECOPD.

Dissociation between transdiaphragmatic pressure and diaphragm thickening. A key and initially counterintuitive observation is that PEEPi,dyn was directly associated with tidal Pdi yet inversely associated with the diaphragm thickening fraction (TF,di). Rather than contradictory, these findings capture complementary aspects of diaphragmatic function. Tidal Pdi expresses the pressure the diaphragm must develop against the prevailing load, whereas TF,di is a geometric index heavily influenced by muscle operating length, curvature, and the extent of the zone of apposition (30). Dynamic hyperinflation shortens the diaphragm along its length–tension relationship, flattens its dome, and reduces the zone of apposition, displacing the muscle to a mechanically disadvantageous portion of its force–length curve (30,31,40,81). Under these conditions, a shortened, flattened diaphragm can still transmit—or be obliged to transmit—a high transdiaphragmatic pressure to overcome the threshold load, while thickening less during contraction. The inverse association we observed between PEEPi,dyn and maximal diaphragmatic pressure-generating capacity (Pdi,sniff) reinforces this interpretation and is consistent with the reduction in maximal diaphragmatic pressure documented as COPD transitions from the stable state to acute exacerbation (32,34). Taken together, the data indicate that the larger tidal Pdi seen at higher PEEPi,dyn reflects a greater pressure requirement imposed on a diaphragm with diminished reserve, and that TF,di and Pdi are not interchangeable surrogates of diaphragmatic effort in hyperinflated patients — an important methodological caveat for bedside ultrasound, where thickening fraction alone may underestimate the true mechanical output of a disadvantaged diaphragm (75,76).

Redistribution of inspiratory effort toward accessory muscles. Respiratory muscle ultrasound provided convergent evidence of an altered load-capacity balance. Higher PEEPi,dyn was associated with lower diaphragm thickening and greater parasternal intercostal (TF,ic) and sternocleidomastoid (TF,scm) thickening, consistent with progressive recruitment of the extra-diaphragmatic and accessory muscles as the diaphragm's contribution becomes mechanically constrained (40,41). The sternocleidomastoid, in particular, is a late-recruited accessory muscle engaged only when inspiratory effort approaches a substantial fraction of maximal inspiratory pressure, so its activation is a marker of an already advanced compensatory state (40). Although the diaphragmatic recruitment index during maximal sniff (TMax,di) tended to rise with PEEPi,dyn, this association was weaker, in keeping with the concept that increasing demand is met predominantly by accessory rather than diaphragmatic

reserve once hyperinflation is established. The coherence between the pressure-derived partitioning (Pes/Pdi ratio, Pga,rise) and the ultrasound recruitment pattern strengthens the interpretation of PEEPi,dyn as an integrated index of mechanical disadvantage rather than an isolated pressure measurement.

Breathing pattern and dyspnea. The mechanical burden translated into a functionally less efficient breathing pattern and a heavier symptom load. Higher PEEPi,dyn was associated with lower expiratory tidal volume (absolute and normalized to predicted body weight), lower mean inspiratory flow, a lower duty cycle, and a higher respiratory rate. Physiologically, when a larger fraction of inspiratory pressure is expended to overcome the threshold load, less effective pressure remains available to generate tidal volume, so patients defend minute ventilation through tachypnea rather than through deeper breaths (16,19). This strategy is self-defeating in flow-limited lungs, because the shortened expiratory time further limits lung emptying and perpetuates air trapping and PEEPi,dyn (16). The direct association between PEEPi,dyn and the modified Borg score links this mechanical inefficiency to the patient's experience and is consistent with the neuromechanical dissociation model of dyspnea in COPD, in which a rising neural drive fails to produce a proportionate ventilatory output (10,36). The simultaneous convergence of pressure, ultrasound, breathing-pattern, and symptom findings around PEEPi,dyn is a central message of this work.

Implications for HFNC. These relationships are particularly relevant to the mechanism of action of HFNC. HFNC improves ventilatory efficiency through upper-airway dead-space washout, delivers warmed and humidified gas that reduces inspiratory resistance, tends to slow the respiratory rate and thereby lengthen expiratory time, and generates a low level of positive airway pressure. However, the external pressure it produces is modest and highly dependent on flow, cannula fit, and mouth opening, and is therefore likely to be insufficient to counterbalance a large PEEPi,dyn in markedly hyperinflated patients (50,82). Non-invasive ventilation, by contrast, delivers an adjustable external PEEP that can partially offset the inspiratory threshold load together with inspiratory pressure support that directly unloads the respiratory muscles, addressing both sides of the load–capacity imbalance (45,46). This mechanistic asymmetry offers a physiological explanation for the heterogeneous response to HFNC reported in hypercapnic ECOPD and is coherent with guidelines and trial evidence that continue to position NIV as first-line support for acute hypercapnic respiratory failure while framing HFNC as an alternative in selected, less severe patients (45,55).

PEEPi,dyn and the early physiological response to HFNC. The longitudinal analysis extends these considerations by showing that baseline dynamic hyperinflation was associated with the quality of the early response to HFNC. Patients with higher baseline PEEPi,dyn tended to show persistence or worsening rather than reduction of inspiratory effort during the first two hours, less favourable changes in tidal volume, and maintenance or exacerbation of PEEPi,dyn. Notably, the strongest longitudinal association was with the change in PTPes/min — the time-integrated, minute-normalized index that best reflects the metabolic cost of breathing — indicating less effective mechanical unloading precisely in the patients who needed it most (53). The concurrent increase in the Pes/Pdi ratio and TMax,di and the decrease in TF,di, in the presence of essentially unchanged per-breath pressure–time products and tidal Pdi, suggest that the rise in minute effort was driven mainly by the breathing-pattern components (rate and timing) rather than by greater pressure generation per breath. This is internally consistent with the reduced tidal volume and shortened expiratory time that sustain dynamic hyperinflation (5), and the accompanying fall in Pdi,sniff points to a widening mismatch between tidal pressure demand and diaphragmatic pressure-generating reserve.

A load–capacity continuum. A small number of patients developed worsening acidosis during HFNC; several of these had among the highest baseline PEEPi,dyn values and already exhibited signs of diaphragmatic dysfunction. Although this observation is descriptive and hypothesis-generating in so small a sample, it is coherent with the overall picture of an unfavourable load–capacity balance in the most hyperinflated patients. Together with our earlier finding that inspiratory effort and accessory muscle recruitment were already elevated in patients who subsequently failed HFNC while diaphragmatic thickening remained relatively preserved (41), these data are compatible with a continuum in which rising drive and mechanical load first trigger compensatory extra-diaphragmatic recruitment and later progress toward neuromechanical uncoupling and overt diaphragmatic failure as the imbalance worsens.

Clinical and monitoring perspective. Direct measurement of PEEPi,dyn requires esophageal and gastric pressure monitoring and dedicated physiological expertise, which limits its routine bedside use (64). Our data suggest that non-invasive surrogates of its consequences—nasal pressure swings, which tracked esophageal effort closely, and respiratory muscle ultrasound, which captured the redistribution of activity — may offer a more readily applicable way to identify patients with a high threshold load and reduced diaphragmatic reserve. Whether PEEPi,dyn, alone or combined with these non-invasive markers, can prospectively identify

patients unlikely to unload adequately on HFNC, and therefore in need of closer monitoring or earlier escalation to NIV, is an important question for future work.

Limitations. Several limitations should be acknowledged. First, the sample size (n = 12), inherent to the invasive physiological design, precludes multivariable adjustment and reduces the precision and stability of the correlation estimates, as reflected by the generally wide bootstrap 95% confidence intervals; individual effect sizes may be overestimated and should be regarded as hypothesis-generating. Second, PEEPi,dyn and Vte were measured during a brief (<2-minute) standardized interruption of HFNC rather than during continuous delivery; although the interruption was deliberately kept short and recording began without a washout period to limit dissipation of the physiological conditions, it may not perfectly reproduce uninterrupted treatment. Third, a single flow rate (40 L/min) was used; higher flows might generate greater external PEEP and more effective dead-space washout and could therefore modify the observed relationships (50,83). Fourth, the absence of a comparator arm (NIV or conventional oxygen) prevents attributing the observed patterns specifically to HFNC rather than to the natural course of the exacerbation. Fifth, the ultrasound characterization of diaphragmatic function relied on thickening fraction and did not include diaphragmatic excursion. Finally, the two-hour window may be too short to capture the full trajectory of respiratory adaptation, and longer observation would be needed to relate these early physiological signals to clinical outcomes such as HFNC failure and the need for escalation.

CONCLUSION

In spontaneously breathing patients with ECOPD treated with HFNC, a higher dynamic intrinsic PEEP was associated with greater inspiratory effort, impaired diaphragmatic mechanics with compensatory recruitment of the extra-diaphragmatic and accessory muscles, a less efficient breathing pattern, and more severe dyspnea. A higher baseline PEEPi,dyn was also associated with a less favourable early physiological response to HFNC, consistent with less effective respiratory unloading in the most hyperinflated patients. These findings support further investigation of PEEPi,dyn — and of non-invasive markers of its physiological consequences — as tools for physiological monitoring and, potentially, for individualizing the choice of non-invasive respiratory support in ECOPD.

References

1. Petrof BJ, Legaré M, Goldberg P, Milic-Emili J, Gottfried SB. Continuous Positive Airway Pressure Reduces Work of Breathing and Dyspnea during Weaning from Mechanical Ventilation in Severe Chronic Obstructive Pulmonary Disease. American Review of Respiratory Disease. 1990 Feb 1;141(2):281–9. doi: 10.1164/ajrccm/141.2.281 PubMed PMID: 2405757.

2. Colaianni-Alfonso N, Herrera F, Flores D, Deana C, Vapireva M, Biasucci DG, et al. Physiological effects and clinical evidence of high-flow nasal cannula during acute exacerbation in COPD patients: A narrative review. PubMed Central. 2024 Dec 19;5(2):127–33. doi: 10.1016/j.jointm.2024.10.005 PubMed PMID: 40241833.

3. Safiri S, Carson-Chahhoud K, Noori M, Nejadghaderi SA, Sullman MJM, Heris JA, et al. Burden of chronic obstructive pulmonary disease and its attributable risk factors in 204 countries and territories, 1990-2019: results from the Global Burden of Disease Study 2019. BMJ. 2022 Jul 27;378. doi: 10.1136/bmj-2021-069679 PubMed PMID: 35896191.

4. Boers E, Barrett M, Su J, Benjafield A, Sinha S, Kaye L, et al. Global Burden of Chronic Obstructive Pulmonary Disease Through 2050. JAMA Network Open. 2023 Dec 7;6(12). doi: 10.1001/jamanetworkopen.2023.46598 PubMed PMID: 38060225.

5. Global Initiative for Chronic Obstructive Lung Disease. *Global Strategy for the Diagnosis, Management, and Prevention of Chronic Obstructive Pulmonary Disease: 2026 Report*. Global Initiative for Chronic Obstructive Lung Disease. https://goldcopd.org/2026-gold-report-and-pocket-guide/

6. Kim V, Aaron SD. What is a COPD exacerbation? Current definitions, pitfalls, challenges and opportunities for improvement. European Respiratory Journal. 2018;52(5):1801261. doi: 10.1183/13993003.01261-2018 PubMed PMID: 30237306.

7. Campos JLL, Ruiz JAJ, Quintana-Gallego E. Epidemiology of COPD Exacerbations. Seminars in Respiratory and Critical Care Medicine. 2026 Feb 23;47(3):252–61. doi: 10.1055/a-2818-1414 PubMed PMID: 41730299.

8. Tonelli R, Michelacci S, Verduri A, Clini E. Physiopathology of Exacerbation of Chronic Obstructive Pulmonary Disease. Seminars in Respiratory and Critical Care Medicine. 2026 Feb 12;47(3):262–7. doi: 10.1055/a-2811-3019 PubMed PMID: 41679730.

9. Ritchie AI, Wedzicha JA. Definition, Causes, Pathogenesis, and Consequences of Chronic Obstructive Pulmonary Disease Exacerbations. Clinics in Chest Medicine. 2020;41(3):421–38. doi: 10.1016/j.ccm.2020.06.007 PubMed PMID: 32800196.

10. O'Donnell DE. COPD exacerbations {middle dot} 3: Pathophysiology. Thorax. 2006 Mar 24;61(4):354–61. doi: 10.1136/thx.2005.041830 PubMed PMID: 16565268.

11. Wang Z, Locantore N, Haldar K, Ramsheh MY, Beech AS, Ma W, et al. Inflammatory Endotype-associated Airway Microbiome in Chronic Obstructive Pulmonary Disease Clinical Stability and Exacerbations: A Multicohort Longitudinal Analysis. American Journal of Respiratory and Critical Care Medicine. 2021;203(12):1488–502. doi: 10.1164/rccm.202009-3448OC PubMed PMID: 33332995.

12. Singh D, Agusti A, Martinez FJ, Papi A, Pavord ID, Wedzicha JA, et al. Blood Eosinophils and Chronic Obstructive Pulmonary Disease: A Global Initiative for Chronic Obstructive Lung Disease Science Committee 2022 Review. American Journal of Respiratory and Critical Care Medicine. 2022;206(1):17–24. doi: 10.1164/rccm.202201-0209PP PubMed PMID: 35737975.

13. Boucher RC. Muco-Obstructive Lung Diseases. New England Journal of Medicine. 2019;380(20):1941–53. doi: 10.1056/NEJMra1813799 PubMed PMID: 31091375.

14. Dunican EM, Elicker BM, Henry T, Gierada DS, Schiebler ML, Anderson W, et al. Mucus Plugs and Emphysema in the Pathophysiology of Airflow Obstruction and Hypoxemia in Smokers. American Journal of Respiratory and Critical Care Medicine. 2021;203(8):957–68. doi: 10.1164/rccm.202006-2248OC PubMed PMID: 33180550.

15. Wan E, et al. Airway Mucus Plugs on Chest Computed Tomography Are Associated with Exacerbations in Chronic Obstructive Pulmonary Disease. American Journal of Respiratory and Critical Care Medicine. 2025;211:814–22. doi: 10.1164/rccm.202403-0632OC PubMed PMID: 39470402.

16. Gibson GJ. Pulmonary hyperinflation a clinical overview. European Respiratory Journal. 1996 Dec 1;9(12):2640–9. doi: 10.1183/09031936.96.09122640 PubMed PMID: 8980982.

17. Cooper CB. The connection between chronic obstructive pulmonary disease symptoms and hyperinflation and its impact on exercise and function. The American Journal of Medicine. 2006;119(10 Suppl 1):21–31. doi: 10.1016/j.amjmed.2006.08.004 PubMed PMID: 16996896.

18. Munshi L, Mancebo J, Brochard L. Noninvasive Respiratory Support for Adults with Acute Respiratory Failure. New England Journal of Medicine. 2022 Nov 2;387(18):1688–98. doi: 10.1056/nejmra2204556 PubMed PMID: 36322846.

19. Ranieri V, Dambrosio M, Brienza N. Intrinsic PEEP and cardiopulmonary interaction in patients with COPD and acute ventilatory failure. European Respiratory Journal. 1996 Jun 1;9(6):1283–92. doi: 10.1183/09031936.96.09061283 PubMed PMID: 8804950.

20. Śliwiński P, Kamiński D, Zieliński J, Yan S. Partitioning of the elastic work of inspiration in patients with COPD during exercise. European Respiratory Journal. 1998 Feb 1;11(2):416–21. doi: 10.1183/09031936.98.11020416 PubMed PMID: 9551747.

21. Parrilla F, Morán I, Roche-Campo F, Mancebo J. Ventilatory Strategies in Obstructive Lung Disease. Seminars in Respiratory and Critical Care Medicine. 2014 Aug 11;35(4):431–40. doi: 10.1055/s-0034-1382155 PubMed PMID: 25111641.

22. Zakynthinos S, Vassilakopoulos T, Zakynthinos E, Mavrommatis AC, Roussos C. Contribution of Expiratory Muscle Pressure to Dynamic Intrinsic Positive End-Expiratory Pressure. American Journal of Respiratory and Critical Care Medicine. 2000 Nov 1;162(5):1633–40. doi: 10.1164/ajrccm.162.5.9903084 PubMed PMID: 11069788.

23. Lessard M, Lofaso F, Brochard L. Expiratory Muscle Activity Increases Intrinsic Positive End-Expiratory Pressure Independently of Dynamic Hyperinflation in Mechanically Ventilated Patients. American Journal of Respiratory and Critical Care Medicine. 1995 Feb 1;151(2):562–9. doi: 10.1164/ajrccm.151.2.7842221 PubMed PMID: 7842221.

24. Loring SH, Garcia-Jacques M, Malhotra A. Pulmonary characteristics in COPD and mechanisms of increased work of breathing. Journal of Applied Physiology. 2009;107(1):309–14. doi: 10.1152/japplphysiol.00008.2009 PubMed PMID: 19359620.

25. Csoma B, Vulpi MR, Dragonieri S, Bentley A, Felton T, et al. Hypercapnia in COPD: Causes, Consequences, and Therapy. Journal of Clinical Medicine. 2022;11(11):3180. doi: 10.3390/jcm11113180 PubMed PMID: 35683563.

26. Barberà JA, Roca J, Ferrer A, Félez MA, Díaz O, Roger N, et al. Mechanisms of worsening gas exchange during acute exacerbations of chronic obstructive pulmonary disease. European Respiratory Journal. 1997;10(6):1285–91. doi: 10.1183/09031936.97.10061285 PubMed PMID: 9192930.

27. MacIntyre NR. Acute Hypercapnic Respiratory Failure in COPD. Respiratory Care. 2023;68(7):973–82. doi: 10.4187/respcare.10560 PubMed PMID: 37353327.

28. Sartori G, Fantin A, Sartori F, Gabarrús A, Crisafulli E, Torres A. Hypercapnia at admission, regardless of acidosis, may worsen the outcome of hospitalised patients with chronic obstructive pulmonary disease exacerbations. Internal and Emergency Medicine. 2026 Feb 9. doi: 10.1007/s11739-026-04279-0 PubMed PMID: 41661467.

29. Gayan-Ramirez G, Decramer M. Mechanisms of striated muscle dysfunction during acute exacerbations of COPD. Journal of Applied Physiology. 2013;114(9):1291–9. doi: 10.1152/japplphysiol.00847.2012 PubMed PMID: 23372146.

30. Troyer AD. Effect of hyperinflation on the diaphragm. European Respiratory Journal. 1997 Mar 1;10(3):708–13. doi: 10.1183/09031936.97.10030708 PubMed PMID: 9073010.

31. López-Rey JM, Beyer B, García-Vargas E, Torres-Sánchez I, García-Río F, Bastir M. Three-dimensional geometric morphometric analysis of diaphragmatic dome motion in COPD patients. The Anatomical Record. 2026 Feb 11. doi: 10.1002/ar.70161 PubMed PMID: 41674160.

32. Similowski T, Yan S, Gauthier AP, Macklem PT, Bellemare F. Contractile Properties of the Human Diaphragm during Chronic Hyperinflation. New England Journal of Medicine. 1991 Sep 26;325(13):917–23. doi: 10.1056/nejm199109263251304 PubMed PMID: 1881417.

33. Ottenheijm CAC, Heunks LMA, Dekhuijzen PNR. Diaphragm muscle fiber dysfunction in chronic obstructive pulmonary disease: toward a pathophysiological concept. American Journal of Respiratory and Critical Care Medicine. 2007;175(12):1233–40. doi: 10.1164/rccm.200701-020PP PubMed PMID: 17413128.

34. Ceriana P, Vitacca M, Carlucci A, Paneroni M, Pisani L, Nava S. Changes of Respiratory Mechanics in COPD Patients from Stable State to Acute Exacerbations with Respiratory Failure. COPD Journal of Chronic Obstructive Pulmonary Disease. 2016 Dec 20;14(2):150–5. doi: 10.1080/15412555.2016.1254173 PubMed PMID: 27997251.

35. O'Donnell DE, Milne KM, James MD, de-Torres JP, Neder JA. Dyspnea in COPD: New Mechanistic Insights and Management Implications. Advances in Therapy. 2019 Oct 30;37(1):41–60. doi: 10.1007/s12325-019-01128-9 PubMed PMID: 31673990.

36. Jolley CJ, Luo Y, Steier J, Rafferty GF, Polkey MI, Moxham J. Neural respiratory drive and breathlessness in COPD. European Respiratory Journal. 2014 Oct 16;45(2):355–64. doi: 10.1183/09031936.00063014 PubMed PMID: 25323229.

37. McKenzie DK, Butler JE, Gandevia SC. Respiratory muscle function and activation in chronic obstructive pulmonary disease. Journal of Applied Physiology. 2009;107(2):621–9. doi: 10.1152/japplphysiol.00163.2009 PubMed PMID: 19390004.

38. De Troyer A, Kirkwood PA, Wilson TA. Respiratory Action of the Intercostal Muscles. Physiological Reviews. 2005;85(2):717–56. doi: 10.1152/physrev.00007.2004 PubMed PMID: 15788709.

39. Hudson AL, Gandevia SC, Butler JE. The effect of lung volume on the co-ordinated recruitment of scalene and sternomastoid muscles in humans. The Journal of Physiology. 2007;584(1):261–70. doi: 10.1113/jphysiol.2007.137240 PubMed PMID: 17690147.

40. Decramer M. Hyperinflation and respiratory muscle interaction. European Respiratory Journal. 1997 Apr 1;10(4):934–41. doi: 10.1183/09031936.97.10040934 PubMed PMID: 9150337.

41. Tabbì L, Marchioni A, Messina J, Bombelli S, Puggioni D, Fantini R, et al. Ultrasound-based evaluation of inspiratory muscle effort in patients with type 2 respiratory failure secondary to exacerbation of chronic obstructive pulmonary disease.

European Journal of Internal Medicine. 2025 Dec 16;145:106649. doi: 10.1016/j.ejim.2025.106649 PubMed PMID: 41407586.

42. Suh ES, Mandal S, Harding R, et al. Neural respiratory drive predicts clinical deterioration and safe discharge in exacerbations of COPD. Thorax. 2015;70(12):1123–30. doi: 10.1136/thoraxjnl-2015-207188 PubMed PMID: 26194996.

43. Goligher EC, Jonkman AH, Dianti J, Vaporidi K, Beitler JR, Patel BK, et al. Clinical strategies for implementing lung and diaphragm-protective ventilation: avoiding insufficient and excessive effort. Intensive Care Medicine. 2020;46(12):2314–26. doi: 10.1007/s00134-020-06288-9 PubMed PMID: 33140181.

44. MacDonald MI, Shafuddin E, King PT, Chang CL, Bardin PG, Hancox RJ. Cardiac dysfunction during exacerbations of chronic obstructive pulmonary disease. The Lancet Respiratory Medicine. 2016;4(2):138–48. doi: 10.1016/S2213-2600(15)00509-3 PubMed PMID: 26781000.

45. Rochwerg B, Brochard L, Elliott M, Hess D, Hill NS, Nava S, et al. Official ERS/ATS clinical practice guidelines: noninvasive ventilation for acute respiratory failure. European Respiratory Journal. 2017 Aug 1;50(2):1602426. doi: 10.1183/13993003.02426-2016 PubMed PMID: 28860265.

46. Guan L, Xu J, He Z, Zha S, Huang Q, Niu J, et al. Efficiency of neural respiratory drive changes during non-invasive ventilation and high-flow nasal cannula oxygen therapy in AECOPD patients with acute hypercapnic respiratory failure: A randomised cross-over study. Annals of Intensive Care. 2026 Jan 1;16:100019. doi: 10.1016/j.aicoj.2025.100019 PubMed PMID: 41788481.

47. Pisani L, Vega ML. Use of Nasal High Flow in Stable COPD: Rationale and Physiology. COPD Journal of Chronic Obstructive Pulmonary Disease. 2017 May 1;14(3):346–50. doi: 10.1080/15412555.2017.1315715 PubMed PMID: 28459282.

48. Oczkowski S, Ergan B, Bos L, Chatwin M, Ferrer M, Gregoretti C, et al. ERS clinical practice guidelines: high-flow nasal cannula in acute respiratory failure. European Respiratory Journal. 2022;59(4):2101574. doi: 10.1183/13993003.01574-2021 PubMed PMID: 34649974.

49. Roca O, Hernández G, Diaz-Lobato S, Carratalá JM, Gutierrez RM, et al. Current evidence for the effectiveness of heated and humidified high flow nasal cannula

supportive therapy in adult patients with respiratory failure. Critical Care. 2016 Apr 19;20(1):109. doi: 10.1186/s13054-016-1263-z PubMed PMID: 27121707.

50. Pinkham MI, Tatkov S. Effect of flow and cannula size on generated pressure during nasal high flow. Critical Care. 2020 May 24;24(1):248. doi: 10.1186/s13054-020-02980-w PubMed PMID: 32448344.

51. Bräunlich J, Mauersberger F, Wirtz H. Effectiveness of nasal highflow in hypercapnic COPD patients is flow and leakage dependent. BMC Pulmonary Medicine. 2018;18(1):14. doi: 10.1186/s12890-018-0576-x

52. Menga LS, Balzani E, Gelormini C, Mastropietro C, Volpe NJ, Signore RS, et al. Physiological effects of noninvasive respiratory support strategies in adults with acute hypoxemic respiratory failure: a systematic review and network meta-analysis. Critical Care. 2025 Oct 28;29(1):456. doi: 10.1186/s13054-025-05670-7 PubMed PMID: 41152956.

53. Delorme M, Bouchard PA, Simon M, Simard S, Lellouche F. Effects of High-Flow Nasal Cannula on the Work of Breathing in Patients Recovering From Acute Respiratory Failure*. Critical Care Medicine. 2017 Aug 29;45(12):1981–8. doi: 10.1097/ccm.0000000000002693 PubMed PMID: 28857852.

54. Cortegiani A, Crimi C, Noto A, Helviz Y, Giarratano A, Gregoretti C, et al. Effect of high-flow nasal therapy on dyspnea, comfort, and respiratory rate. Critical Care. 2019 Jun 5;23(1):201. doi: 10.1186/s13054-019-2473-y PubMed PMID: 31167660.

55. Tan D, Wang B, Cao P, Wang Y, Wang Y, Sun J, et al. High flow nasal cannula oxygen therapy versus non-invasive ventilation for acute exacerbations of chronic obstructive pulmonary disease with acute-moderate hypercapnic respiratory failure: a randomized controlled non-inferiority trial. Critical Care. 2024 Jul 18;28(1):250. doi: 10.1186/s13054-024-05040-9 PubMed PMID: 39026242.

56. Pantazopoulos I, Boutlas S, Mavrovounis G, et al. Nasal high flow or noninvasive ventilation? Navigating hypercapnic COPD exacerbation treatment: A randomized noninferiority clinical trial. Respiratory Medicine. 2024;232:107762. doi: 10.1016/j.rmed.2024.107762 PubMed PMID: 39111544.

57. RENOVATE Investigators and the BRICNet Authors, Francio F, Weigert RM, et al. High-Flow Nasal Oxygen vs Noninvasive Ventilation in Patients With Acute

Respiratory Failure: The RENOVATE Randomized Clinical Trial. *JAMA*. 2025;333(10):875. doi:10.1001/jama.2024.26244

58. Tonelli R, Fantini R, Bruzzi G, et al. Effect of high flow nasal oxygen on inspiratory effort of patients with acute hypoxic respiratory failure and do not intubate orders. Internal and Emergency Medicine. 2024;19(2):333–42. doi: 10.1007/s11739-023-03471-w PubMed PMID: 38158462.

59. Vitacca M, Ceriana P, Prediletto I, Carlucci A, Paneroni M, Ambrosino N, et al. Intrinsic Dynamic Positive End-Expiratory Pressure in Stable Patients with Chronic Obstructive Pulmonary Disease. Respiration. 2020 Jan 1;99(12):1129–35. doi: 10.1159/000511266 PubMed PMID: 33271563.

60. Yan S, Kayser B. Differential Inspiratory Muscle Pressure Contributions to Breathing during Dynamic Hyperinflation. American Journal of Respiratory and Critical Care Medicine. 1997 Aug 1;156(2):497–503. doi: 10.1164/ajrccm.156.2.9611073 PubMed PMID: 9279230.

61. Mauri T, Yoshida T, Bellani G, Goligher EC, Carteaux G, Rittayamai N, et al. Esophageal and transpulmonary pressure in the clinical setting: meaning, usefulness and perspectives. Intensive Care Medicine. 2016 Jun 22;42(9):1360–73. doi: 10.1007/s00134-016-4400-x PubMed PMID: 27334266.

62. Akoumianaki E, Maggiore SM, Valenza F, et al. The Application of Esophageal Pressure Measurement in Patients with Respiratory Failure. American Journal of Respiratory and Critical Care Medicine. 2014;189(5):520–31. doi: 10.1164/rccm.201312-2193CI PubMed PMID: 24467647.

63. Tonelli R, Fantini R, Tabbì L, et al. Early Inspiratory Effort Assessment by Esophageal Manometry Predicts Noninvasive Ventilation Outcome in De Novo Respiratory Failure. A Pilot Study. American Journal of Respiratory and Critical Care Medicine. 2020;202(4):558–67. doi: 10.1164/rccm.201912-2512OC PubMed PMID: 32325004.

64. Mojoli F, Torriglia F, Orlando A, Bianchi I, Arisi E, Pozzi M. Technical aspects of bedside respiratory monitoring of transpulmonary pressure. Annals of Translational Medicine. 2018 Oct 1;6(19):377. doi: 10.21037/atm.2018.08.37 PubMed PMID: 30460251.

65. Tonelli R, Cortegiani A, Marchioni A, Fantini R, Tabbì L, Castaniere I, et al. Nasal pressure swings as the measure of inspiratory effort in spontaneously breathing patients with de novo acute respiratory failure. Critical Care. 2022 Mar 24;26(1):70. doi: 10.1186/s13054-022-03938-w PubMed PMID: 35331323.

66. Tonelli R, Cortegiani A, Fantini R, et al. Accuracy of Nasal Pressure Swing to Predict Failure of High-Flow Nasal Oxygen in Patients with Acute Hypoxemic Respiratory Failure. American Journal of Respiratory and Critical Care Medicine. 2023;207(6):787–9. doi: 10.1164/rccm.202210-1848LE PubMed PMID: 36476122.

67. Tonelli R, Bruzzi G, Fantini R, Tabbì L, Moretti A, Livrieri F, et al. Assessment of nasal pressure swing predicts respiratory support dependency in patients with hypoxic respiratory failure. European Journal of Internal Medicine. 2025. doi: 10.1016/j.ejim.2025.02.016 PubMed PMID: 40057383.

68. Goligher EC, Laghi F, Detsky ME, Farías P, Murray A, Brace D, et al. Measuring diaphragm thickness with ultrasound in mechanically ventilated patients: feasibility, reproducibility and validity. Intensive Care Medicine. 2015 Feb 18;41(4):642–9. doi: 10.1007/s00134-015-3687-3 PubMed PMID: 25693448.

69. Marchioni A, Castaniere I, Tonelli R, et al. Ultrasound-assessed diaphragmatic impairment is a predictor of outcomes in patients with acute exacerbation of chronic obstructive pulmonary disease undergoing noninvasive ventilation. Critical Care. 2018;22(1):109. doi: 10.1186/s13054-018-2033-x PubMed PMID: 29703214.

70. Dres M, Dubé B, Goligher EC, Vorona S, Demiri S, Morawiec É, et al. Usefulness of Parasternal Intercostal Muscle Ultrasound during Weaning from Mechanical Ventilation. Anesthesiology. 2020 Feb 21;132(5):1114–25. doi: 10.1097/aln.0000000000003191 PubMed PMID: 32084029.

71. Formenti P, Umbrello M, Dres M, Chiumello D. Ultrasonographic assessment of parasternal intercostal muscles during mechanical ventilation. Annals of Intensive Care. 2020;10(1):120. doi: 10.1186/s13613-020-00735-y PubMed PMID: 32894372.

72. Rittayamai N, Marinpong V, Chuaychoo B, Tscheikuna J, Brochard LJ. Ultrasound Evaluation of Parasternal Intercostal, Diaphragm Activity, and Their Ratio in Male Patients with Chronic Obstructive Pulmonary Disease. American Journal of

Respiratory and Critical Care Medicine. 2024;209(8):1016–8. doi: 10.1164/rccm.202310-1769LE PubMed PMID: 38319129.

73. Shiraishi M, Higashimoto Y, Sugiya R, et al. Sternocleidomastoid Muscle Thickness Correlates with Exercise Tolerance in Patients with COPD. Respiration. 2023;102(1):64–73. doi: 10.1159/000527100 PubMed PMID: 36412608.

74. Umbrello M, Formenti P, Lusardi AC, et al. Oesophageal pressure and respiratory muscle ultrasonographic measurements indicate inspiratory effort during pressure support ventilation. British Journal of Anaesthesia. 2020;125(1):e148–57. doi: 10.1016/j.bja.2020.02.026 PubMed PMID: 32386831.

75. Poulard T, Bachasson D, Fossé Q, Niérat MC, Hogrel JY, Demoule A, et al. Poor Correlation between Diaphragm Thickening Fraction and Transdiaphragmatic Pressure in Mechanically Ventilated Patients and Healthy Subjects. Anesthesiology. 2021 Nov 17;136(1):162–75. doi: 10.1097/aln.0000000000004042 PubMed PMID: 34788380.

76. Rittayamai N, Chuaychoo B, Tscheikuna J, Dres M, Goligher EC, Brochard L. Ultrasound Evaluation of Diaphragm Force Reserve in Patients with Chronic Obstructive Pulmonary Disease. Annals of the American Thoracic Society. 2020 Jul 2;17(10):1222–30. doi: 10.1513/annalsats.202002-129oc PubMed PMID: 32614240.

77. Vries H de, Jonkman AH, Shi Z, Man A, Heunks L. Assessing breathing effort in mechanical ventilation: physiology and clinical implications. Annals of Translational Medicine. 2018 Oct 1;6(19):387. doi: 10.21037/atm.2018.05.53 PubMed PMID: 30460261.

78. Fantini R, Mandrioli J, Zona S, Antenora F, Iattoni A, Monelli M, et al. Ultrasound assessment of diaphragmatic function in patients with amyotrophic lateral sclerosis. Respirology. 2016 Mar 19;21(5):932–8. doi: 10.1111/resp.12759 PubMed PMID: 26994409.

79. Cala SJ, Kenyon CM, Lee A, Watkin K, Macklem PT, Rochester DF. Respiratory Ultrasonography of Human Parasternal Intercostal Muscle In Vivo. Ultrasound in Medicine & Biology. 1998;24(3):313–26. doi: 10.1016/S0301-5629(97)00271-8

80. Truong D, Abo S, Whish-Wilson GA, et al. Methodological and Clinimetric Evaluation of Inspiratory Respiratory Muscle Ultrasound in the Critical Care Setting:

A Systematic Review and Meta-Analysis. Critical Care Medicine. 2023;51(2):e24–36. doi: 10.1097/CCM.0000000000005739

81. Boriek AM, Rodriguez-Santiago N, Kim SH, Ford AL, Wynd S, Hubmayr RD. Compromised pressure-generating capacity of diaphragmatic muscle and its interaction with the lower rib cage at high lung volume during airway occlusion. American Journal of Physiology-Regulatory, Integrative and Comparative Physiology. 2025 Oct 24;329(6). doi: 10.1152/ajpregu.00080.2025 PubMed PMID: 41134675.

82. Gotti M, Umbrello M, Sabbatini G, Mantovani EA, Foggetti L, Menozzi A, et al. The Impact of High-Flow Nasal Cannula Therapy on Diaphragmatic Function Assessed by Ultrasound: A Pilot Clinical Study. Critical Care Medicine. 2025 Dec 19;54(3):435–43. doi: 10.1097/ccm.0000000000006994 PubMed PMID: 41416853.

83. Mauri T, Turrini C, Eronia N, Grasselli G, Volta CA, Bellani G, et al. Physiologic Effects of High-Flow Nasal Cannula in Acute Hypoxemic Respiratory Failure. American Journal of Respiratory and Critical Care Medicine. 2017 Mar 6;195(9):1207–15. doi: 10.1164/rccm.201605-0916oc PubMed PMID: 27997805.